Regulation of Maximal Open Probability Is a Separable Function of $Ca_v\beta$ Subunit in L-type Ca^{2+} Channel, Dependent on NH_2 Terminus of α_{1C} ($Ca_v1.2\alpha$)

Nataly Kanevsky and Nathan Dascal

Department of Physiology and Pharmacology, Sackler School of Medicine, Tel Aviv University, Ramat Aviv 69978, Israel

β subunits ($Ca_v\beta$) increase macroscopic currents of voltage-dependent Ca^{2+} channels (VDCC) by increasing surface expression and modulating their gating, causing a leftward shift in conductance–voltage (G-V) curve and increasing the maximal open probability, $P_{o,max}$. In L-type $Ca_v1.2$ channels, the $Ca_v\beta$-induced increase in macroscopic current crucially depends on the initial segment of the cytosolic NH_2 terminus (NT) of the $Ca_v1.2\alpha$ (α_{1C}) subunit. This segment, which we term the "NT inhibitory (NTI) module," potently inhibits long-NT (cardiac) isoform of α_{1C} that features an initial segment of 46 amino acid residues (aa); removal of NTI module greatly increases macroscopic currents. It is not known whether an NTI module exists in the short-NT (smooth muscle/brain type) α_{1C} isoform with a 16-aa initial segment. We addressed this question, and the molecular mechanism of NTI module action, by expressing subunits of $Ca_v1.2$ in *Xenopus* oocytes. NT deletions and chimeras identified aa 1–20 of the long-NT as necessary and sufficient to perform NTI module functions. Coexpression of β_{2b} subunit reproducibly modulated function and surface expression of α_{1C}, despite the presence of measurable amounts of an endogenous $Ca_v\beta$ in *Xenopus* oocytes. Coexpressed β_{2b} increased surface expression of α_{1C} approximately twofold (as demonstrated by two independent immunohistochemical methods), shifted the G-V curve by ~14 mV, and increased $P_{o,max}$ 2.8–3.8-fold. Neither the surface expression of the channel without $Ca_v\beta$ nor β_{2b}-induced increase in surface expression or the shift in G-V curve depended on the presence of the NTI module. In contrast, the increase in $P_{o,max}$ was completely absent in the short-NT isoform and in mutants of long-NT α_{1C} lacking the NTI module. We conclude that regulation of $P_{o,max}$ is a discrete, separable function of $Ca_v\beta$. In $Ca_v1.2$, this action of $Ca_v\beta$ depends on NT of α_{1C} and is α_{1C} isoform specific.

INTRODUCTION

Voltage-dependent Ca^{2+} channels are grouped into three families, Ca_v1–Ca_v3 (Ertel et al., 2000). The main structural component of all Ca_v channels is the α_1 subunit that bears the archetypal features of a voltage-dependent channel, with four membrane-spanning domains and a large cytosolic domain comprising the NH_2- and $COOH$-terminal parts of the protein (NT and CT, respectively), and three large intracellular loops, L1–L3, connecting the membrane-spanning domains (Fig. 1 A). In addition, members of Ca_v1 and Ca_v2 families also contain at least two auxiliary subunits, β ($Ca_v\beta1$–$Ca_v\beta4$) and $\alpha_2\delta$ (Isom et al., 1994; Varadi et al., 1995; De Waard et al., 1996; Birnbaumer et al., 1998; Walker and De Waard, 1998; Striessnig, 1999; Catterall, 2000). The $\alpha_2\delta$ subunit regulates channel expression and trafficking to the plasma membrane (PM) (Shistik et al., 1995; Yasuda et al., 2004; Canti et al., 2005), increases the open probability (P_o) of α_{1C} (Shistik et al., 1995), and regulates some pharmacological properties of the channel (De Waard et al., 1996). $Ca_v\beta$ subunits are modular MAGUK-type proteins with an SH_3-like and a guanylate kinase (GK)-like domain (Chen et al., 2004; McGee et al., 2004; Opatowsky et al., 2004;

Van Petegem et al., 2004). The latter binds with high affinity to a conserved AID (α-interaction domain) motif within the first intracellular loop (L1) of α_1 (Pragnell et al., 1994). The β subunits profoundly modulate the properties of voltage-dependent Ca^{2+} channels. The most prominent effect is a great increase in the magnitude of macroscopic Ca^{2+} currents, caused by the expression of $Ca_v\beta$ on top of α_1 or $\alpha_1+\alpha_2\delta$ in most heterologous expression systems (Mori et al., 1991; Singer et al., 1991; Varadi et al., 1991; Williams et al., 1992; Castellano et al., 1993; Lory et al., 1993), or by the expression of $Ca_v\beta$ in cardiac cells (Wei et al., 2000; Colecraft et al., 2002). Accordingly, depletion or elimination of endogenous $Ca_v\beta$ subunits by knockdown/knockout strategies greatly reduces voltage-dependent Ca^{2+} currents in various excitable cells (Gregg et al., 1996; Strube et al., 1996; Leuranguer et al., 1998; Namkung et al., 1998; Chu et al., 2004).

Extensive studies in heterologous expression systems revealed a multitude of effects of β subunits on

Abbreviations used in this paper: aa, amino acid; AID, α-interaction domain; CT, COOH terminus; HA, hemagglutinin; HEK, human embryonic kidney; NT, NH_2 terminus; NTI, NT inhibitory; PM, plasma membrane; P_o, open probability; VDCC, voltage-dependent calcium channel; VDI, voltage-dependent inactivation.

biosynthesis and gating of VDCCs. First, $Ca_v\beta$ increases the surface expression of α_1, by improving its trafficking from the ER to the PM (Chien et al., 1995; Brice et al., 1997; Tareilus et al., 1997; Gao et al., 1999), probably by relieving an ER retention signal (Bichet et al., 2000). Second, $Ca_v\beta$ regulates several gating properties of VDCCs. The extent of regulation varies among subtypes and isoforms of $Ca_v\beta$ and $Ca_v\alpha_1$. The most prominent changes in macroscopic currents include hyperpolarizing (leftward) shifts in current–voltage (I-V) (or conductance–voltage, G-V) and steady-state inactivation curves, an increase in the rate of activation, and changes in the kinetics of voltage-dependent inactivation (for reviews see Birnbaumer et al., 1998; Stotz and Zamponi, 2001; Dolphin, 2003). The shift in G-V curve reflects an improved coupling between gating charge movement and channel opening (Neely et al., 1993, 2004). On the single channel level, coexpression of $Ca_v\beta$ increases the open probability, P_o, without changing the single channel conductance (Wakamori et al., 1993; Shistik et al., 1995; Costantin et al., 1998).

The overall increase in macroscopic Ca^{2+} channel currents caused by heterologous expression of $Ca_v\beta$ results both from increased surface expression, and from changes in gating that lead to increased P_o. Regulation of trafficking by $Ca_v\beta$ is clearly separable from modulation of gating; changes in trafficking and gating occur on distinct time and $Ca_v\beta$ concentration scales, and mutations that disrupt the high-affinity interaction between AID and $Ca_v\beta$ disrupt colocalization of α_1 and β in the PM and membrane targeting of α_1, but spare some or all of the β-induced changes in gating parameters. Thus, the high-affinity binding of $Ca_v\beta$ to AID is obligatory for the regulation of trafficking but not gating (Yamaguchi et al., 1998; Canti et al., 1999, 2001; Gerster et al., 1999; Hullin et al., 2003; McGee et al., 2004; Leroy et al., 2005; Maltez et al., 2005). The SH_3–GK domain interaction may also play an important role in regulating trafficking (Takahashi et al., 2005). Among gating effects of $Ca_v\beta$, at least one, the regulation of kinetics of voltage-dependent inactivation (VDI), is separable from the others. A palmitoylated isoform of β_{2a} (usually designated simply as β_{2a}) decelerates the VDI of several $Ca_v\alpha$, whereas all other β subunits, including a nonpalmitoylated isoform of β_{2a} (np-β_{2a} of rabbit, and its human orthologue β_{2b}), accelerate VDI. At the same time, the enhanced trafficking of α_1 and the hyperpolarizing shift in G-V curve are independent of palmitoylation of $Ca_v\beta$ (Olcese et al., 1994; Chien et al., 1996; Qin et al., 1996, 1998; Gao et al., 1999). The separability of different effects of $Ca_v\beta$ implies that they are determined by distinct molecular interactions between different parts of β and/or α_1. Some actions of β may rely upon low-affinity interactions of β (the SH_3 domain in particular) with regions outside the AID in α_1, either in L1 or in the CT in some types of α_1 (Tareilus et al., 1997; Walker et al., 1999;

Takahashi et al., 2004; Maltez et al., 2005). At present, it is unclear whether gating effects of $Ca_v\beta$ other than change in kinetics are also separable, and what is the molecular basis of separate effects of $Ca_v\beta$ on different gating parameters.

It is notable that cells most widely used for heterologous expression of Ca^{2+} channels, *Xenopus* oocytes and human embryonic kidney (HEK) cells, contain small but measurable amounts of an endogenous $Ca_v\beta$ protein that undoubtedly aids the "β-less" channels to reach the PM (Tareilus et al., 1997; Canti et al., 2001; Leroy et al., 2005). Arguably, the presence of a minimal amount of endogenous $Ca_v\beta$ may be obligatory for surface expression of at least some subtypes of Ca_v1 and Ca_v2 channels (Tareilus et al., 1997; Leroy et al., 2005). An absence of such endogenous $Ca_v\beta$ may explain the reports that in some cell lines transfected with α_{1C} alone or even with $\alpha_{1C}+\alpha_2\delta$, no functional Ca^{2+} channel expression is observed (Gao et al., 1999; Harry et al., 2004; Kobrinsky et al., 2004). The presence of the endogenous $Ca_v\beta$, which is permissive for trafficking of α_1 to PM, does not impair the ability of coexpressed or exogenously added $Ca_v\beta$ protein to modulate the biophysical properties of the channel (Tareilus et al., 1997; Yamaguchi et al., 1998; Garcia et al., 2002). Therefore, it has been proposed that the endogenous β only "chaperones" α_1, helping it to leave the ER without staying with it in the PM; the added exogenous β then binds to α_1 and modulates the gating (the single $Ca_v\beta$-binding model). An alternative multiple $Ca_v\beta$-binding model contends that the endogenous β remains irreversibly bound to AID, and additional β subunit(s) modulate channel gating by interacting with other parts of α_1 (discussed by Birnbaumer et al., 1998; Jones, 2002; Dolphin, 2003). A recent study that used a β_{2b} subunit tethered to the end of α_{1C} strongly supports a functional 1:1 α_1-β stoichiometry (Dalton et al., 2005); unfortunately, not all functions of β were fully recovered by the tethered β, leaving this fundamental issue open for argument.

Unfortunately, the exact extent of regulation of different Ca_v channels by various $Ca_v\beta$ is still debated (discussed in Yasuda et al., 2004), and the contribution of different mechanisms to the increase in whole-cell current has not yet been precisely assessed. The variations are aggravated by apparent inconsistencies between results obtained in different cells and the use of different isoforms of $Ca_v\alpha_1$ and $Ca_v\beta$. To properly understand the molecular principles underlying the different actions of $Ca_v\beta$, one needs to reliably monitor both the surface expression of α_1 and a defined set of gating parameters, in a well characterized system. In this report, we implemented such an approach to analyze the mechanism of regulation of $Ca_v1.2$ (α_{1C}), the L-type channel present in most excitable tissues, by β_{2b}. The study focused on the parameters of channel activity that lead to changes in the magnitude of the macroscopic Ba^{2+} current (I_{Ba}),

leaving the regulation of inactivation out of scope. We have previously found that in the cardiac (long-NT) isoform of α_{1C}, the first 46 aa of the cytosolic NT constitute an NH_2-terminal inhibitory (NTI) module whose removal greatly increases the macroscopic current and the P_o. The presence of the NTI module is also crucial for β_{2b}-induced increase in I_{Ba} via the long-NT isoform α_{1C} in *Xenopus* oocytes. We therefore proposed that the β subunit acts, in part, by functionally counteracting the inhibitory effect of this module (Shistik et al., 1998; Ivanina et al., 2000). Here we demonstrate that the long-NT initial segment selectively regulates a single action of β_{2b}: the elevation of $P_{o,max}$. This modulation is absent in deletion mutants lacking the initial NT segment, and in a short-NT isoform of α_{1C} (smooth muscle/brain subtype), in which the initial 46 aa encoded by exon 1a are replaced by a partially homologous stretch of 16 aa encoded by exon 1. Other effects of β (trafficking, G-V curve shift) are preserved. This is the first report on a discrete regulation by $Ca_v\beta$ of $P_{o,max}$ in $Ca_v1.2$. These findings bear upon the isoform-specific physiological properties of the L-type Ca^{2+} channel and upon the physiological role of $Ca_v\beta$ in different tissues.

MATERIALS AND METHODS

DNA Constructs and mRNA

cDNAs of rabbit heart α_{1C} (X15539), rabbit heart np-β_{2a} (L06110) (here termed β_{2b}), skeletal muscle $\alpha_2\delta$-1 (P13806) subunits, and the α_{1C} NH_2-terminal truncation mutants $\alpha_{1C}\Delta5$, $\alpha_{1C}\Delta20$, $\alpha_{1C}\Delta46$, and $\alpha_{1C}\Delta139$ were prepared and used as described previously (Shistik et al., 1998). The mutants $\Delta6$-20, $\Delta21$-46, $T_{10}A/Y_{13}F/P_{15}A$, NT_{SL}, and NT_{LS} chimeras were constructed by standard PCR methods. To create α_{1C}-HA, the hemagglutinin (HA) tag (*SR*YPYDVPDYA; the first two amino acids SR were added in order to create an XbaI restriction site in the corresponding cDNA sequence) has been inserted into the extracellular loop after the S5 transmembrane segment of α_{1C}-wt, between amino acids Q713 and T714, by two consecutive PCRs. The $\Delta21$-46-HA and NT_{LS}-HA were then produced by standard subcloning procedures. All mutations and PCR products were verified by nucleotide sequencing at the Tel Aviv University Sequencing Facility.

All cDNA constructs of α_{1C} and mutants were inserted into the same vector, pGEM-HE-GSB (Shistik et al., 1998), which is a derivative of pGEM-HE (Liman et al., 1992). This vector provides the necessary 5' and 3' untranslated regions (UTR) from *Xenopus* α-globin. Therefore, only the coding sequences of all α_{1C} derivatives, without any residual original UTRs, were inserted into the vector. To minimize any variability that may be caused by variations in quality and quantity of RNAs, in each series of experiments all tested RNAs (all mutants of α_{1C} under study and the wt α_{1C}) were synthesized anew on the same day.

Oocyte Culture and Electrophysiology

All the experiments were performed in accordance with the Tel Aviv University Institutional Animal Care and Use Committee (permits no. 11–99-47 and 11–05-064). *Xenopus laevis* frogs were maintained and operated, and oocytes were collected, defolliculated, and injected with RNA as previously described (Dascal and Lotan, 1992). In brief, female frogs, maintained at $20 \pm 2°C$ on an 11-h light/13-h dark cycle, were anaesthetized in a 0.15% solution

of procaine methanesulfonate (MS222), and portions of ovary were removed through a small incision on the abdomen. The incision was sutured, and the animal was returned to a separate tank until it had fully recovered from the anesthesia, and afterwards was returned to a large tank where, together with the other postoperational animals, it was allowed to recover for at least 4 wk until the next surgery. The animals did not show any signs of postoperational distress. The oocytes were injected with the mRNAs of α_{1C} or its mutants, $\alpha_2\delta$, and β_{2b}, according to the design of experiment (0.3–5 ng for electrophysiology and 2.5–5 ng for imaging). Unless indicated otherwise, equal amounts (by weight) of different RNAs were injected. The oocytes were incubated for 3–5 d at 20–22°C in ND96 solution (96 mM NaCl, 2 mM KCl, 1 mM $MgCl_2$, 1 mM $CaCl_2$, 5 mM HEPES, pH 7.5) supplemented with 2.5 mM Na-pyruvate and 50 μg/ml gentamycin. In some batches with high endogenous chloride currents, oocytes were injected with 25–30 nl/oocyte of the Ca^{2+} chelator EGTA (50–100 mM), giving a final concentration of 2–5 mM within the oocyte (assuming oocyte's free water volume of 0.5 μl).

Whole cell currents were recorded using the Gene Clamp 500 amplifier (Axon Instruments) using the two-electrode voltage clamp technique, in a solution containing 40 mM $Ba(OH)_2$, 50 mM NaOH, 2 mM KOH, and 5 mM HEPES, titrated to pH 7.5 with methanesulfonic acid (Shistik et al., 1995). Stimulation, data acquisition, and analysis were performed using pCLAMP software (Axon Instruments). Current–voltage (I-V) relation of Ba^{2+} currents was measured by 60-ms, 10-mV steps given every 10 s from a holding potential of -80 mV. In each cell, the net I_{Ba} was obtained by subtraction of the residual currents recorded with the same protocols after applying 200 μM Cd^{2+}.

Immunocytochemistry and Confocal Imaging

Immunocytochemistry in giant PM patches was done essentially as previously described (Singer-Lahat et al., 2000; Peleg et al., 2002), as illustrated in Fig. 3. Oocytes were devitellinized by peeling off the vitelline membrane in ND96, and placed on plastic coverslips (Thermanox plastic coverslip; Nunc). After sticking to the coverslip, the oocyte was removed mechanically and/or by washing with a strong jet of solution. Pieces of membranes strongly attached to the coverslip were continuously washed until the membrane patch became transparent without any visible cytosolic content and pigment granules. After fixation for 10 min in 1% formaldehyde, the membranes were washed three times with 1% BSA dissolved in TBS solution (135 mM NaCl, 10 mM Tris-HCl, pH 7.4). Blocking of nonspecific binding sites was done with donkey immunoglobulin G (IgG, whole molecule, 1/200, Jackson ImmunoResearch Laboratories) for 30 min. Each coverslip was incubated for 1 h with CT4 antibody against α_{1C} COOH terminus (1:500; provided by M. Hosey, Northwestern University, Chicago, IL; see Gao et al., 2001) or against L2 (1:500; Alomone Labs.). Residual antibody was washed out with 1% BSA three times, 5 min each. This was followed by a 30-min incubation with secondary antibody (Cy3 donkey anti–rabbit IgG, 1:400; Jackson Immuno-Research Laboratories). Free secondary antibody was then washed out with 1% BSA three times, 5 min each in darkness and the coverslips were mounted on a glass slide. The fluorescent labeling was examined by a confocal laser scanning microscope (LSM 410 or LSM 510, Zeiss, Germany). 40× NA/1.2 C-apochromat water-immersion lens (Axiovert 135 M, Zeiss) was used for imaging. The Cy3-conjugated secondary antibody was excited at 488 nm and the emitted light at >568 nm was collected. The fluorescent signals were analyzed by measuring total luminosity (optical density) of the whole image using the Tina 2.1 (Raytest Isotopenmelgerilte GmbH) or Carl Zeiss MicroImaging, Inc. LSM5 software. In all confocal imaging procedures, care was taken to completely avoid saturation of the signal. The gain of the photomultiplier was kept <75% of maximum. In each experiment, all oocytes from the

different groups were studied using a constant set of imaging parameters. The normalized intensities were always calculated relative to the control group of the same experiment. Net fluorescence intensity per unit area was obtained by subtracting an averaged background signal measured in the same way in membranes of native (uninjected) oocytes from the same batch.

Immunocytochemistry and imaging of whole oocytes has been done as follows. 3–4 d after the injection of RNA, the oocytes were fixated in 4% formaldehyde (37%) in Ca-free ND96 solution for 15 min. Blocking of nonspecific binding sites was done by 5% skim milk for 1 h. Then the oocytes were incubated for 1 h with the mouse monoclonal IgG_{2a} antibody against HA (Santa Cruz Biotechnology), diluted 1:400 in 2.5% skim milk. Residual antibody was washed out with 2.5% skim milk three times, 5 min each. This was followed by 1 h incubation with the secondary antibody (Alexa-conjugated anti–mouse IgG, 1:400; Jackson ImmunoResearch Laboratories) in dark. Free secondary antibody was then washed out with Ca-free ND96. Oocytes were placed in a chamber with a transparent bottom, and fluorescence imaging of optical slices was performed with LSM 510 ($\times 20$ objective, zoom = 1, pinhole 3 Airy units). Alexa was excited at 594 nm and the emitted light was collected using long-pass (LP) 615-nm filter. The fluorescent signals were usually analyzed as described in Fig. 4 D. Alternatively, the intensity of fluorescence in the PM was measured by averaging the signal obtained from six standard circular regions of interest. Net fluorescence intensity per unit area was obtained by subtracting the background signal measured in native oocytes.

Data Analysis

Current–voltage (I-V) curve was fitted to the Boltzmann equation in the form

$$I_{Ba} = G_{max}(V_m - V_{rev})/(1 + \exp(-(V_m - V_{1/2})/K_a)), \quad (1)$$

where K_a is the slope factor, $V_{1/2}$ is the voltage that causes half maximal activation, G_{max} is the maximal macroscopic conductance, V_m is membrane voltage, I_{Ba} is the current measured at the same voltage, and V_{rev} is the reversal potential of I_{Ba}. The obtained parameters of G_{max} and V_{rev} were then used to calculate fractional conductance at each V_m, G/G_{max}, using the equation

$$G/G_{max} = I_{Ba}/(G_{max}(V_m - V_{rev})), \quad (2)$$

where G is the total macroscopic conductance at V_m. The conductance–voltage (G-V) curves were plotted with the values of $V_{1/2}$ and K_a obtained from the fit of the I-V curves, using the following form of the Boltzmann equation:

$$G/G_{max} = 1/(1 + \exp(-(V_m - V_{1/2})/K_a)). \quad (3)$$

The results were summarized from many groups of oocytes from different donors ("batches"). To avoid series resistance artifacts associated with very large currents (Schreibmayer et al., 1994), or inaccuracies resulting from a contribution from the small endogenous oocyte's Ca^{2+}, Cl^-, or K^+ channel currents when the macroscopic I_{Ba} was low (mainly in oocytes expressing $\alpha_{1C} + \alpha_2\delta$ without β_{2b}; Dascal, 1987; Dascal et al., 1992), these quantitative analyses were performed only in experiments in which, at the peak of the I-V curve, $0.1\ \mu A \leq I_{Ba} \leq 6\ \mu A$.

The calculation of changes in $P_{o,max}$ was based on the following considerations. The total macroscopic conductance, estimated by measuring peak currents at different voltages, is a linear function of P_o:

$$G = \gamma \times N \times P_o, \quad (4)$$

where γ is the single channel conductance, and N is the total number of functional channels in the PM (Hille, 2002). In Ca_v channels, P_o is voltage dependent whereas γ and N are not. P_o reaches a maximal value, $P_{o,max}$, at positive voltages where a maximal macroscopic conductance, G_{max}, is attained. Both G_{max} and $P_{o,max}$ are empirical parameters that are considered voltage independent and are interrelated as follows:

$$P_{o,max} = G_{max}/(\gamma \times N). \quad (5)$$

The fold change in N caused by a treatment, R_N, is defined as $N_{treatment}/N_{control}$. From here, if γ is constant, the change in $P_{o,max}$ caused by a treatment is given by

$$(6)$$

$$\text{Fold change in } P_{o,max}$$
$$= P_{o,max(treatment)}/P_{o,max(control)} = (G_{max(treatment)}/G_{max(control)}/R_N).$$

In this study, R_N was monitored by imaging measurements in giant PM patches or in whole oocytes. Eq. 6 is similar to those used previously (Wei et al., 1994; Takahashi et al., 2004) to assess changes in P_o; in these studies, R_N was estimated from the measurement of Q_{max} (the maximal gating charge).

To compare parameters (I_{40}, surface α_{1C} labeling, or G_{max}) observed or calculated in oocytes of different batches, data from individual cells were averaged across batches using the following normalization procedure (Sharon et al., 1997). The value of the parameter in each cell was normalized to the mean value of this parameter in the control group of the same batch. This procedure was also applied to the cells of the control group, thus providing a useful measure of variability in this group and enabling an accurate statistical analysis. Normalized values were then averaged from all cells across all batches. The results are presented as means ± SEM Multiple group comparisons were done by one-way analysis of variance (ANOVA) test followed by Tukey's test. Two-group comparisons were done using Student's t test.
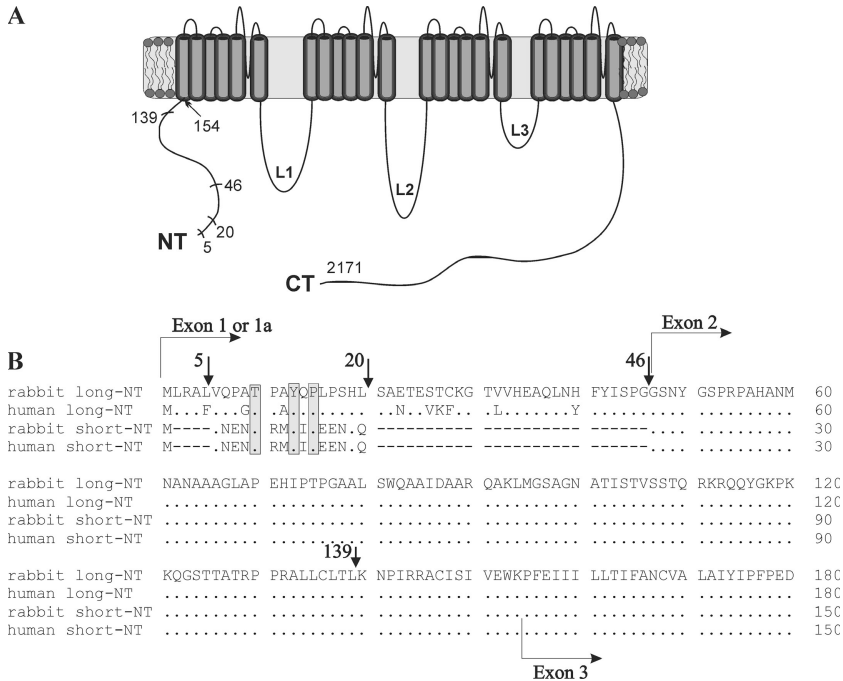
Online Supplemental Material

Table S1 (available at http://www.jgp.org/cgi/content/full/jgp.200609485/DC1) shows the mean values of G_{max} and V_{rev} obtained in Boltzmann equation fits for some of the α_{1C} constructs used in this study.

RESULTS

Mapping the Part of NT Crucial for the Regulation of G_{max}

Deletions of initial segment of long-NT α_{1C} increase the amplitude of I_{Ba} but attenuate the current enhancement caused by $Ca_v\beta$. It is not known if the same structural elements of NT alter both macroscopic currents and modulation by $Ca_v\beta$. To address this problem, we sought to delineate the regions that are important for these modulations. Fig. 1 B shows the protein sequences of the NH_2-terminal part of long-NT and short-NT isoforms of rabbit and human α_{1C} (the corresponding sequences in rat and mouse are also highly homologous; see Blumenstein et al., 2002). The cytosolic NT consists of 124 (short-NT) or 154 aa (long-NT), which are the products of transcription of alternative initial exons 1 or 1a, respectively, and an invariable exon 2 encoding 108 aa. Amino acids 6–20 of the long-NT show partial homology with the first 16 aa of the short-NT

A

139 — 154

L1

L2

L3

NT 5 20 46

CT 2171

B

```
                  Exon 1 or 1a                                    Exon 2
                      5↓              20↓                    46↓
rabbit long-NT   MLRALVQPAT PAYQPLPSHL SAETESTCKG TVVHEAQLNH FYISPGGSNY GSPRPAHANM   60
human long-NT    M...F...G. .A........ ..N..VKF.. .L........Y .......... ..........   60
rabbit short-NT  M----.NEN. RM.I.EEN.Q ---------- ---------- ------.... ..........   30
human short-NT   M----.NEN. RM.I.EEN.Q ---------- ---------- ------.... ..........   30

rabbit long-NT   NANAAAGLAP EHIPTPGAAL SWQAAIDAAR QAKLMGSAGN ATISTVSSTQ RKRQQYGKPK  120
human long-NT    .......... .......... .......... .......... .......... ..........  120
rabbit short-NT  .......... .......... .......... .......... .......... ..........   90
human short-NT   .......... .......... .......... .......... .......... ..........   90

                                      139↓
rabbit long-NT   KQGSTTATRP PRALLCLTLK NPIRRACISI VEWKPFEIII LLTIFANCVA LAIYIPFPED  180
human long-NT    .......... .......... .......... .......... .......... ..........  180
rabbit short-NT  .......... .......... .......... .......... .......... ..........  150
human short-NT   .......... .......... .......... .......... .......... ..........  150
                                                 Exon 3
```

Figure 1. The structure of the α_{1C} subunit and its NH$_2$ terminus. (A) Schematic presentation of the α_{1C} subunit of the L-type Ca^{2+} channel, Ca$_v$1.2. Numbering is shown according to rabbit long-NT α_{1C}-wt (Mikami et al., 1989). The principal NH$_2$-terminal deletion mutants used in this work are indicated by short lines. (B) Comparison of protein sequences of NH$_2$ termini of rabbit and human long-NT and short-NT isoforms. Dots stand for full sequence homology, dashes show gaps, and shaded areas show the conserved motif TxxYxP. Arrows indicate the location of the inserted methionine at the beginning of each NH$_2$-terminal deletion mutant. The initial segments of long-NT and short-NT isoforms are encoded by exons 1a and exon 1, accordingly; the beginning of the transmembrane segment IS1 corresponds to the beginning of exon 3.

(Shistik et al., 1998); in particular, the amino acids T_{10}, Y_{13}, and P_{15} (which we call TxxYxP motif; numbering by long-NT) are conserved in both isoforms (Fig. 1 B, gray boxes). In the previous studies, we have created several NT deletion mutants of rabbit cardiac long-NT α_{1C}. The logic of these deletions was dictated by the comparison of nucleotide sequences of long- and short-NT isoforms. Initially, we deleted amino acid stretches from the first methionine up to the positions corresponding to the boundaries of the region of partial homology (mutants $\alpha_{1C}\Delta5$ and $\alpha_{1C}\Delta20$), and then up to the beginning of the high homology region ($\alpha_{1C}\Delta46$). We also deleted almost all of the cytosolic part of the NT ($\alpha_{1C}\Delta139$). In the previous studies, only $\alpha_{1C}\Delta46$ and $\alpha_{1C}\Delta139$ have been characterized in detail; voltage-dependent characteristics, protein expression levels, and the effect of β subunit have not been compared systematically in most mutants. Such a comparative study has been done in the experiments described below. In addition, we have deleted the region of partial homology with short-NT α_{1C}, aa 6–20, from long-NT α_{1C} (mutant $\alpha_{1C}\Delta6$-20). We also mutated the TxxYxP motif, creating the $T_{10}A/Y_{13}F/P_{15}A$ ($\alpha_{1C}TYP$) mutant.

To delineate the region of long-NT that regulates the magnitude of I_{Ba}, either long-NT wild-type α_{1C} (α_{1C}-wt) or the various NT deletion mutants were expressed without Ca$_v\beta$. The expression of α_{1C}-wt alone in *Xenopus* oocytes results in very small (a few nA) Ba^{2+} currents that are difficult to reliably resolve and analyze, and often difficult to separate from currents via oocyte's endogenous Ca$_v$ channels, which are non–L type (Singer et al., 1991; Dascal et al., 1992; Singer-Lahat et al., 1994). Therefore, $\alpha_2\delta$ was coexpressed in all experiments. The latter greatly increases I_{Ba} compared with α_{1C}-wt alone, but does not increase the current via the endogenous channels. $\alpha_2\delta$ aids trafficking α_{1C} to the PM (Shistik et al., 1995; Yasuda et al., 2004; Canti et al., 2005) and produces certain synergistic (more than additive) effects with some β subunits (Singer et al., 1991; Yamaguchi et al., 2000), but most of the actions of β_{2b} are similar in the presence or absence of $\alpha_2\delta$ (see Table IV). In oocytes expressing $\alpha_{1C}+\alpha_2\delta$ or $\alpha_{1C}+\alpha_2\delta+\beta_{2b}$, the contribution of endogenous channels to I_{Ba} was negligible; I_{Ba} was reduced by >95% by 10 µM of the dihydropyridine L-type Ca^{2+} channel blockers nitrendipine and nifedipine (Singer-Lahat et al., 1994; unpublished data).

Fig. 2 A shows the routine experimental protocol used to analyze the I-V characteristic of the expressed channels. Ca^{2+} channel currents were elicited by 60-ms depolarizing pulses from a holding potential of −80 mV, in 10-mV steps, in a solution containing 40 mM Ba^{2+} using the two-electrode voltage clamp technique. Net I_{Ba} was obtained by subtracting currents elicited by the same voltage protocol in the presence of 200 µM CdCl$_2$ (Fig. 2 A, left). The absolute amplitude of I_{Ba} depended on the amount of RNA injected, period of incubation, and also varied among oocyte batches. The amount of the injected RNA (of both α_{1C}-wt and $\alpha_2\delta$) varied in our experiments between 1 and 5 ng/oocyte, depending on the experimental design. In this range, greater amounts of RNA always resulted in larger I_{Ba}. The right panel of Fig. 2 A shows a typical I-V curve of net I_{Ba}, averaged from six oocytes of the same batch (donor frog). Without Ca$_v\beta$, I_{Ba} was maximal at ∼30 mV. In the following, to compare I_{Ba} across different groups and treatments,

we chose to use the value of I_{Ba} measured at $+40$ mV (I_{40}) rather than at the peak of the I-V curve, because the latter varied between different treatments. Also, at $+40$ mV, the whole-cell Ba^{2+} conductance is close to maximum under most conditions (Figs. 2 and 4), therefore changes in I_{40} should approximately reflect changes in G_{max}.

As reported previously (Shistik et al., 1999), in the $\alpha_{1C}\Delta5$ mutant, I_{40} increased about twofold compared with α_{1C}-wt, without any significant change in the voltage dependence of activation (Fig. 2 B). The calculated increase in G_{max} in the $\alpha_{1C}\Delta5$ mutant was 66% (Table II). In comparison, the deletion of 20 or more aa of the long-NT initial segment caused a robust seven to ninefold increase in I_{40} and in the calculated G_{max} (Fig. 2, Ba and Ca, and Table II). For a summary of the absolute values of G_{max} in the different groups, injected with the same RNA amount of 1 ng/oocyte, see Table S1 (available at http://www.jgp.org/cgi/content/full/jgp.200609485/DC1).

As reported earlier (Wei et al., 1996; Shistik et al., 1998), the I-V curves in $\alpha_{1C}\Delta46$ and $\alpha_{1C}\Delta139$ appeared similar to α_{1C}-wt. However, an exhaustive comparison of a large amount of records revealed a small hyperpolarizing shift caused by the NT deletions, as illustrated in normalized averaged I-V curves (Fig. 2 Cb). To assure that the shift was not an artifact resulting form a larger current amplitude in the NT deletion mutants, in two batches (14–16 oocytes) oocytes were injected with amounts of RNA adjusted to produce I_{Ba} of similar amplitude in α_{1C}-wt, $\alpha_{1C}\Delta46$, and $\alpha_{1C}\Delta20$. The I-V curve shift was observed in all cases. Fitting I-V curves to Boltzmann equation (solid lines in Fig. 2 Cb) indicated a statistically significant 5–7 mV shift in the half activation voltage, $V_{1/2}$, in all NT deletion mutants studied except $\alpha_{1C}\Delta5$ (Table I). The leftward shift in the G-V curves is more clearly seen in conductance–voltage (G-V) curves that were drawn through the data points using the Boltzmann equation parameters obtained in I-V curve fits (Fig. 2 Cc). In addition, the slope appears to be increased by the NT deletions. Indeed, the slope factor K_a was slightly but statistically significantly reduced, from 9.6 mV in α_{1C}-wt to $\sim$7.9 mV in most mutants (Table I). None of the mutations caused any changes in the reversal potential of I_{Ba} (see Table S1).

The robust increase in I_{Ba} and the shift in G-V curve were also observed in the $\alpha_{1C}\Delta6$-20 mutant lacking the 16 aa of the partial homology region. Mutation of the conserved TxxYxP motif produced similar but milder changes (Fig. 2 and Table I). The changes in G_{max} (calculated from the Boltzmann fits) were similar to changes in the measured I_{40} (Table II). Taken together, these data imply that amino acids 6–20 of the long-NT isoform constitute a crucial part of the NTI module. The increase in I_{Ba} and in G_{max} is accompanied by a moderate hyperpolarizing shift in the G-V curve; this
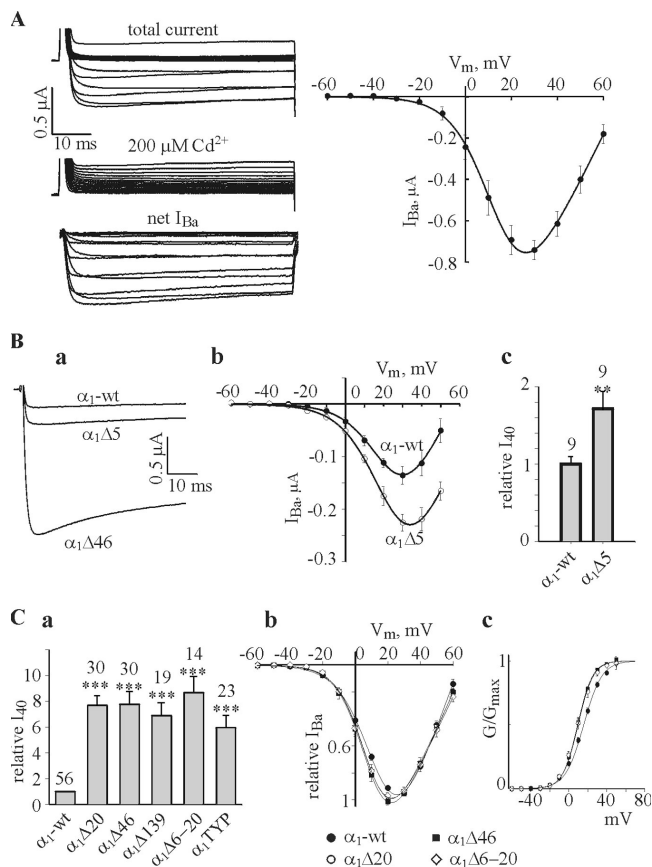
Figure 2. Effects of NH_2-terminal deletions and $T_{10}A/Y_{13}F/P_{15}A$ mutation on I_{Ba} in the absence of $Ca_v\beta$ (the $\alpha_{1C}\alpha_2\delta$ subunit composition). (A) The standard procedure used to monitor I_{Ba}, and an averaged I-V curve. See explanations in the text. (B) Comparison of I_{Ba} in α_{1C}-wt and $\alpha_{1C}\Delta5$ (2.5 ng RNA/oocyte of each subunit). Panel a shows representative current traces recorded at $+40$ mV in oocytes of one batch (donor). A current trace obtained in an oocyte expressing the $\alpha_1\Delta46$ mutant is shown for comparison. Panel b shows averaged I-V curves from α_{1C}-wt and $\alpha_1\Delta5$ groups ($n = 9$ oocytes, $N = 2$ batches). The normalized values of I_{40} are shown in panel c. (C) Panel a shows the summary of relative I_{40} in the various mutants. I_{40} in each oocyte was normalized to the average I_{40} of α_{1C}-wt of the same batch, as explained in Materials and Methods. Panels b and c show normalized I-V and G-V curves, respectively, of the indicated channel constructs, averaged from oocytes of two representative batches ($n = 8$–14, $N = 2$). Amount of injected RNA was varied from 0.3 ng/oocyte in NT mutants to 5 ng/oocyte in α_1-wt to reach comparable I_{Ba} amplitudes in order to minimize the fitting artifacts. Note that Boltzmann fits have been performed separately in each oocyte. For illustration purposes, in averaged I-V and G-V curves shown in C and in the following figures, the solid lines through averaged experimental points were drawn using Boltzmann equation with values of $V_{1/2}$ and K_a from Table I. In this and the following figures, the numbers above bars indicate the number of cells tested, and asterisks indicate statistically significant differences, as follows: *, $P < 0.05$; **, $P < 0.01$; ***, $P < 0.001$.

effect is also fully dependent on the presence of the same 16 aa. The $T_{10}A/Y_{13}F/P_{15}A$ mutation interferes with the function of the NTI module by a mechanism yet to be determined.

TABLE I

Effects of NT Deletions and Mutations of α_{1C} on the Gating Parameters of Ba^{2+} Current Activation

	$V_{1/2}$, mV		K_a, mV	
Construct	No β_{2b}	With β_{2b}	No β_{2b}	With β_{2b}
α_{1C}-wt	15.66 ± 1.23 (56)	1.49 ± 0.79 (56)[d]	9.62 ± 0.31 (56)	7.2 ± 0.13 (56)[d]
$\alpha_1\Delta5$	15.83 ± 3.17 (6)	0.91 ± 0.37 (9)[d]	9.48 ± 0.92 (6)	5.59 ± 0.08 (9) [b,d]
$\alpha_1\Delta20$	9.28 ± 0.98 (19)[b]	-1.14 ± 1.14 (19)[d]	7.87 ± 0.18 (19)[b]	6.41 ± 0.23 (19)[b,d]
$\alpha_1\Delta46$	9.49 ± 0.99 (30)[b]	-1.40 ± 0.80 (20)[d]	7.88 ± 0.24 (30)[b]	5.87 ± 0.18 (20)[b,d]
$\alpha_1\Delta139$	11.02 ± 1.00 (16)[a]	-1.83 ± 3.58 (13)[d]	7.93 ± 0.15 (16)[b]	5.38 ± 0.35 (13)[b,d]
$\alpha_1\Delta6\text{-}20$	8.61 ± 1.56 (8)	-1.28 ± 2.21 (14)[c]	7.83 ± 0.23 (8)	6.29 ± 0.23 (14)[b,d]
α_1TYP	10.28 ± 0.94 (23)[b]	-2.36 ± 0.57 (12)[d]	8.88 ± 0.24 (23)	6.13 ± 0.27 (12)[b,d]
α_{1C}-short	9.83 ± 1.28 (22)[b]	-2.19 ± 1.20 (26)[d]	7.15 ± 0.28 (22)[b]	6.06 ± 0.19 (26)[b,c]
$\alpha_1\Delta21\text{-}46$	20.75 ± 1.73 (9)	5.68 ± 1.93 (12)[d]	9.15 ± 0.33 (9)	6.94 ± 0.11 (12)[d]
NT_{SL}	9.77 ± 1.40 (13)[a]	-1.89 ± 2.59 (18)[d]	8.03 ± 0.17 (13)[b]	5.95 ± 0.3 (18)[b,d]
NT_{LS}	13.86 ± 2.18 (13)	-3.59 ± 2.9 (9)[d]	6.58 ± 0.97 (13)[b]	4.45 ± 0.62 (9)[b,c]
HA-labeled constructs				
α_{1C}-HA	17.88 ± 0.59 (6)	1.43 ± 1.38 (6)[d]	8.53 ± 0.21 (6)	6.55 ± 0.27 (6)[d]
$\alpha_{1C}\Delta21\text{-}46\text{-}HA$	18.37 ± 1.08 (7)	3.6 ± 1.16 (6)[d]	8.34 ± 0.39 (7)	6.8 ± 0.17 (6)[d]
NT_{SL}-HA	7.12 ± 1.67 (6)[b]	-3.06 ± 1.54 (6)[d]	6.76 ± 0.4 (6)[b]	4.89 ± 0.49 (6)[a,d]

The values of $V_{1/2}$ and K_a were obtained in each cell by fitting the I-V curve to the Boltzmann equation (Eq. 1 in Materials and Methods). Mean $\pm$ SEM are shown, with numbers of cells in parentheses.

[a]Statistically significant difference in $V_{1/2}$ or K_a as compared with α_{1C}-wt (or α_{1C}-HA) by one-way ANOVA followed by the Dunnett's test. $P < 0.05$.

[b]Statistically significant difference in $V_{1/2}$ or K_a as compared with α_{1C}-wt (or α_{1C}-HA) by one-way ANOVA followed by the Dunnett's test. $P < 0.01$.

[c]Statistically significant difference compared to no β_{2b} group by t test. $P < 0.01$.

[d]Statistically significant difference compared to no β_{2b} group by t test. $P < 0.001$.

Previously, controversial results have been reported regarding the surface expression of α_{1C} with NT deletions of 40 aa or more from a long-NT α_{1C}, expressed in *Xenopus* oocytes. Wei et al. (1996) reported an approximately sixfold increase in surface expression on the basis of measurements of Q_{max} in cut-open oocytes. In contrast, we did not observe any changes in surface expression in $\alpha_{1C}\Delta46$ either by counting channels in cell-attached patches, or by immunoprecipitating α_{1C} from manually separated plasma membranes (Shistik et al., 1998). Here we confirm these results by an independent imaging method (Singer-Lahat et al., 2000; Peleg et al., 2002). Proteins expressed in the PM were visualized by immunostaining in giant membrane patches in which the cytosolic surface of the PM is exposed to external solution (Fig. 3 A). The membrane protein in the patch is labeled with an antibody against a cytosolic segment, then with a fluorescently labeled secondary antibody, and visualized using a confocal microscope (see Materials and Methods for details). The image captures a randomly selected 105×105 μm area within a (larger) patch. The large size of the imaged area ensures a fair averaging of channel density even if the channels are clustered. Patches from many tens of oocytes can be screened during a 1-d experiment, providing statistically reliable data. This is a big advantage over the previously employed method of immunoprecipitation of α_{1C} from manually separated PM of metabolically labeled oocytes (Shistik et al., 1995, 1998), which produced one experimental point for 20–30 whole-oocyte membranes.

Fig. 3 B shows images of representative membrane patches from oocytes of one batch expressing α_{1C}-wt or various NT mutants of α_{1C} without the β subunit. The antibody labeling was clearly detected in all channel constructs, and no significant labeling was observed in uninjected oocytes at these imaging parameters. The data from two oocyte batches are summarized in Fig. 3 Ca, showing that there were no significant differences in the expression of any of the channel variants tested. This result was reproduced later in a separate series of experiments (see Fig. 4, A and B) and also using an alternative imaging method (see Fig. 7 C). At the same time, I_{Ba} measured in oocytes of one of these two batches was enhanced by the NT mutations, as usual (Fig. 3 Cb). We conclude that physical or functional removal of the NTI module of the long NH_2 terminus does not alter the surface expression of α_{1C}. Since the single channel conductance is not changed either (Shistik et al., 1998), all of the increase in G_{max} caused by these mutations must result from an increase in $P_{o,max}$. Indeed, calculations using Eq. 6 show that all these mutations cause a greater than sixfold increase in $P_{o,max}$ (Table II), except $\alpha_{1C}\Delta5$, which shows only a 37% increase. The increase in I_{40} was essentially identical (Table II).

Regulation by β_{2b} Subunit of $P_{o,max}$, But Not of Other Parameters, Depends on NT of α_{1C}

We used the nonpalmitoylated np-β_{2a} (Hullin et al., 1992), which is the rabbit orthologue of human β_{2b} (96% identity), the most abundant cardiac β subunit in
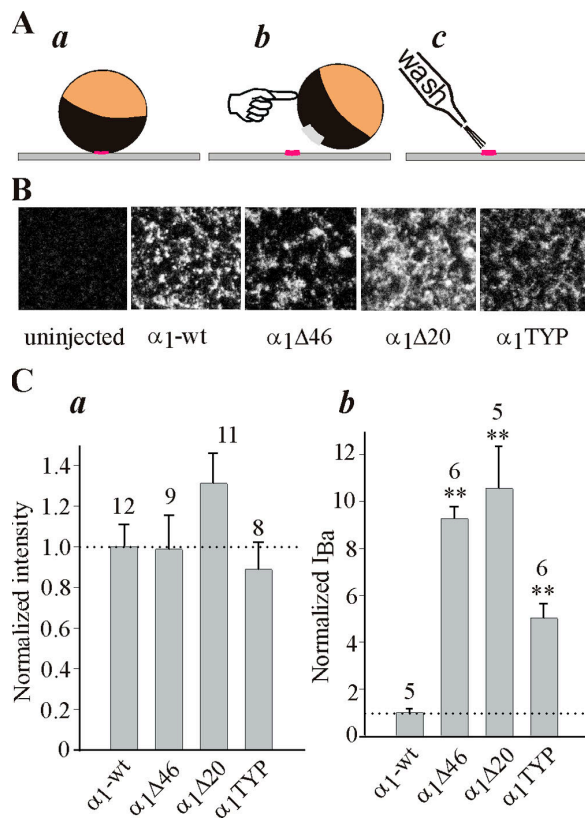
Figure 3. NT mutations and deletions do not alter the surface expression of α_{1C}. (A) A simplified presentation of the method used to measure the surface expression of α_{1C} in giant membrane patches (see Materials and Methods for details). A devitellinized intact oocyte is placed for 10–20 min on coverslip with its animal (dark) hemisphere facing the coverslip (a). After attachment, the oocyte is swept away and patches of membrane (usually >100 μm in diameter) remain stuck to the coverslip (b). The cytosolic surface of the PM, facing the external solution, is thoroughly washed until the membrane appears transparent (c) and then stained with an antibody directed against a cytosolic part of the channel. (B) Examples of confocal images of α_{1C}-wt, $\alpha_{1C}\Delta46$, $\alpha_{1C}\Delta20$, and α_{1C}TYP in giant patches of oocytes of the same batch. (C) NT mutations do not alter the surface expression of α_{1C} (a), despite the typical differences in I_{Ba} (measured at +20 mV) in oocytes of one of these batches (b). The amount of injected RNA was 5 ng/oocyte.

rat and humans (Colecraft et al., 2002; Hullin et al., 2003). To avoid confusion between palmitoylated and nonpalmitoylated forms of β_{2a}, we refer to np-β_{2a} as β_{2b}. Unlike the palmitoylated splice variant isoform (β_{2a}) of the same gene, β_{2b} does not slow down the VDI and does not reside in PM in the absence of α_{1C} (Olcese et al., 1994; Chien et al., 1998). When expressed in *Xenopus* oocytes, β_{2b} accelerates the VDI of Ca$_v$1.2, and in addition causes a robust increase in the whole-cell current and affects all gating parameters (Hullin et al., 1992; Shistik et al., 1995). However, it is not clear whether coexpression of either β_{2a} or β_{2b} improves the trafficking of α_{1C} to the PM in *Xenopus* oocytes. No change (Neely et al., 1993, 2004) or a mild ~50%

increase (Shistik et al., 1995) have been reported (see Table IV and Discussion).

Using the imaging method shown in Fig. 3, we have examined the effect of coexpression of β_{2b} on the amount of α_{1C}-wt, $\alpha_{1C}\Delta20$, $\alpha_{1C}\Delta46$, and α_{1C}TYP in two to four batches of oocytes; $\alpha_2\delta$ was always coexpressed (Fig. 4). As before, in the absence of Ca$_v\beta$, the surface expression of NT mutants was similar to that of α_{1C}-wt (Fig. 4, A and B). In contrast, β_{2b} induced a mild but reproducible and statistically significant ~70% increase (P < 0.001) in the surface expression in all α_{1C} constructs (Fig. 4, A and C).

The effect of β_{2b} on surface expression of α_{1C} was additionally verified using an independent method, using a modified α_{1C} (termed α_{1C}-HA) with an extracellular HA tag inserted in the extracellular loop following the S5 segment of domain I. A similar construct was previously used to study the trafficking of α_{1C} in mammalian cells (Altier et al., 2002). Ba^{2+} currents via channels formed by α_{1C}-HA, coexpressed with α_2/δ with or without β_{2b}, did not differ in amplitude or voltage dependency from α_{1C}-wt (unpublished data; Table I). Surface expression of the HA label was measured using a confocal microscope in whole intact oocytes fixated with formaldehyde and treated with an anti-HA antibody and a secondary antibody conjugated to a fluorescent dye (Fig. 4 D). As shown in Fig. 4 Da, the expression of β_{2b} caused a clear increase in surface expression of α_{1C}-HA. The results were quantified as explained in Fig. 4 legend, and showed a 2.09 ± 0.34-fold increase in the intensity of fluorescence caused by β_{2b} (Fig. 4 Dc). This estimate, though somewhat higher than by measuring the effect of β_{2b} in giant PM patches, was not significantly different when compared in the same oocyte batch (not depicted). These results unequivocally demonstrate that, despite the theoretical possibility that some of the fluorescent signal in the giant membrane patches arises from α_{1C} found in submembrane ER, the latter method provides a realistic estimate of α_{1C} levels in the PM. We conclude that, despite the presence of an endogenous Ca$_v\beta$ in the oocytes, the expressed β_{2b} further increases the surface expression of Ca$_v$1.2 channels about twofold (in the presence of $\alpha_2\delta$). The ability of β_{2b} to do so is not affected by the elimination of the NTI module.

Coexpression of β_{2b} also increased the macroscopic currents in wt and all NT mutants. Examples are shown in Fig. 5 A for α_{1C}-wt and $\alpha_{1C}\Delta46$. Note that β_{2b} accelerated the inactivation kinetics in both cases, despite the fact that without Ca$_v\beta$, they were already faster in $\alpha_{1C}\Delta46$ than in α_{1C}-wt. This was a recurrent result in most mutants (unpublished data). Thus, although VDI is out of the scope of this paper, and although it is clear that the NH$_2$ terminus itself plays a role in VDI (see also Shistik et al., 1998; Kobrinsky et al., 2004), we construe that the elimination of the NTI module does not impair the ability of β_{2b} to speed up the VDI.

Relative Changes in Surface Expression, G_{max}, I_{40}, and P_o in NT Mutants in $\alpha_{1C}+\alpha_2/\delta$ Subunit Composition in the Absence of $Ca_v\beta$

Construct	Fold increase in PM α_{1C} labeling	Fold increase in G_{max}	Fold increase in I_{40}	Fold increase in P_o from G_{max}	from I_{40}
α_{1C}-wt	1 ± 0.05 (40; 7)	1 ± 0.04 (56; 11)	1 ± 0.07 (56; 11)		
$\alpha_{1C}\Delta5$	1.21 ± 0.18 (6; 2)	1.66 ± 0.08^c (9; 2)^a	1.76 ± 0.24^b (9; 2)^a	1.37	1.45
$\alpha_{1C}\Delta20$	1.22 ± 0.12 (24; 3)	7.64 ± 0.98^d (30; 6)	7.68 ± 0.34^d (30; 6)	6.26	6.3
$\alpha_{1C}\Delta46$	0.99 ± 0.12 (16; 3)	7.63 ± 0.81^d (30; 6)	7.75 ± 0.95^d (30; 6)	7.7	7.82
$\alpha_{1C}\Delta139$	Not examined	6.81 ± 0.93^d (19; 5)	6.88 ± 0.94^d (19; 5)		
α_{1C}TYP	0.86 ± 0.1 (17; 3)	5.71 ± 0.93^d (23; 3)	5.95 ± 0.95^d (23; 3)	6.63	6.91
$\alpha_{1C}\Delta6$-20	Not examined	8.22 ± 1.01^d (14; 3)	8.6 ± 1.23^d (14; 3)		
α_{1C}-short	1.16 ± 0.14 (9; 2)	8.56 ± 0.98^d (12; 2)	8.71 ± 1.71^d (12; 2)	7.38	7.5
NT_{SL}	1.13 ± 0.19 (11; 2)	5.77 ± 0.56^d (16; 3)	5.98 ± 0.74^d (16; 3)	5.1	5.3
HA-labeled constructs					
α_{1C}-HA	1 ± 0.12 (10; 1)	1 ± 0.11 (9; 3)	1 ± 0.31 (9; 3)		
NT_{LS}-HA	1.15 ± 0.09 (11; 1)	13.6 ± 1.85^d (15; 3)	14.08 ± 2.0^d (15; 3)	11.8	12.2
$\alpha_{1C}\Delta21$-46-HA	0.88 ± 0.09 (11; 1)	1.41 ± 0.29^d (9; 3)	1.47 ± 0.29^d (9; 3)	1.6	1.67

Surface expression was measured by confocal imaging of immunostained α_{1C} in giant membrane patches or, for HA-labeled constructs, in intact oocytes. Numbers in parentheses indicate n; N (the total number of oocytes and the number of oocyte batches tested). To calculate fold change in a parameter, normalization procedure was performed as described in Materials and Methods. Statistical comparisons were performed using one way ANOVA (multiple comparisons versus control group, α_{1C}-wt or α_{1C}-HA, in oocytes injected with the same amount of RNA, followed by Tukey's test).

^{a}In two batches where α_{1C}-wt and $\alpha_{1C}\Delta5$ were compared, the statistical analysis has been done separately from other batches, since the amount of injected RNA was 2.5 ng per oocyte rather than 1 ng. Averaged normalized fold increase in G_{max} and I_{40} for α_{1C}-wt in these two batches was 1 ± 0.16 ($n = 9$, $N = 2$) and 1 ± 0.2 ($n = 9$, $N = 2$), respectively. The statistical analysis was done using t test.
^{b}P < 0.05.
^{c}P < 0.01.
^{d}P < 0.001.

The I-V curves of all α_{1C} mutants, and of the α_{1C}-wt, were shifted to the left by coexpression of β_{2b}. Examples of averaged I-V curves of oocytes from representative batches are shown in Fig. 5 B, and a full summary of normalized I-V and G-V curves averaged from all oocytes is presented in Fig. 5 (C and D). The hyperpolarizing shift produced by β_{2b} is observed both in α_{1C}-wt and in all mutants lacking the NTI module. A closer examination of the results of Boltzmann fits in Table I reveals that the net change in $V_{1/2}$ and K_a parameters caused by β_{2b} in α_{1C}-wt (14 and 2.4 mV, respectively) was somewhat greater than in some of the NT mutants (11–13 and 1.5–2 mV). However, these differences are small and may be within the experimental or fitting error. In all, we conclude that elimination of NT inhibitory module does not impair the ability of β_{2b} to cause a hyperpolarizing shift in the voltage dependency of channel activation.

In contrast to parameters considered so far, the extent of increase in I_{Ba} and in G_{max} caused by coexpression of β_{2b} was altered dramatically by NT mutations (Figs. 5 B, Fig. 6, and Table III). In agreement with previous reports regarding $\alpha_{1C}\Delta20$, $\alpha_{1C}\Delta46$, and $\alpha_{1C}\Delta139$ (Shistik et al., 1998, 1999), all mutations that impaired the function of the NTI module also greatly reduced the ability of β_{2b} to increase I_{Ba} (Fig. 6, A and B). The differences were more pronounced at less positive potentials, because at least part of the increase in I_{Ba} at

these potentials is due to the leftward shift in the I-V curve, as illustrated in Fig. 6 A for some of the mutants. However, even at +40 mV, the difference between α_{1C}-wt and the various mutants is still very substantial (Fig. 6 B). The β_{2b}-induced increase in the calculated G_{max}, which in α_{1C}-wt was 4.65 ± 0.39-fold, was diminished to only 1.92 ± 0.23-fold in $\alpha_{1C}\Delta46$ (P < 0.01; Table III). A similar, though slightly milder, reduction was observed in $\alpha_{1C}\Delta20$ and α_{1C}TYP (Table III). The only outlier is $\alpha_{1C}\Delta5$. The β_{2b}-induced change in I_{40} was even greater in this mutant than in α_{1C}-wt, as measured in two batches of oocytes (Fig. 6 C). This is at odds with a previous observation (Fig. 2 F in Shistik et al., 1999), but a comprehensive investigation into the reasons of controversy is not possible, because in the experiment reported in 1999, the effect of β_{2b} was studied only marginally (Shistik et al., 1999); I_{Ba} was measured only at +10 mV, and no analysis of voltage dependency has been performed. Thus, dose-dependent or batch-dependent effects of β_{2b} on $\alpha_{1C}\Delta5$ cannot be excluded at present.

To summarize, the main conclusion from these experiments is that the ability of β_{2b} to increase G_{max} is greatly reduced by the removal of a crucial part of the NT inhibitory module, aa 6–20. The unique aa 2–5 of the long-NT channel are a part of the NTI module, since their removal already causes a mild increase in $P_{o,max}$; however, it also potentiates the enhancing effect
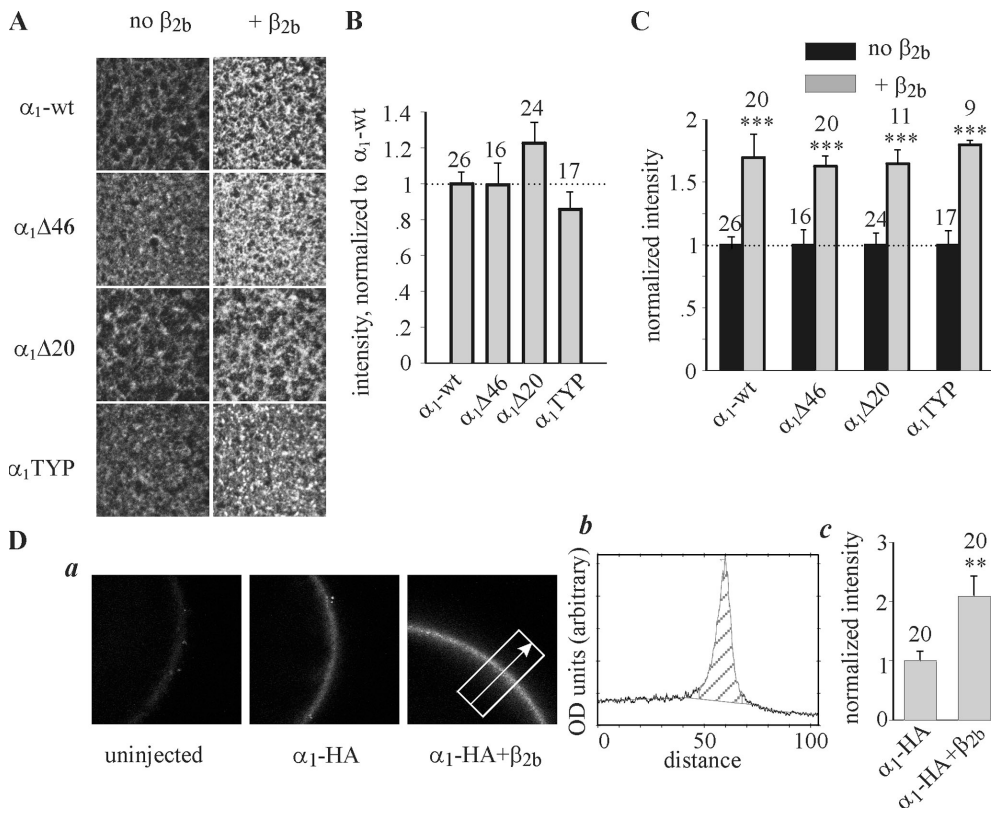
Figure 4. Coexpression of β_{2b} increases the surface expression of α_{1C}-wt and of NT mutants. (A) Examples of confocal images of α_{1C}-wt, $\alpha_{1C}\Delta46$, $\alpha_{1C}\Delta20$, and α_{1C}TYP in giant PM patches, in absence and presence of β_{2b} subunit. (B) Surface expression of the mutant proteins in $\alpha_1\alpha_2\delta$ subunit composition, without β_{2b}, normalized to α_{1C}-wt. This series of experiments included two oocyte batches and was separate from that shown in Fig. 3. Injected RNA was 5 ng/oocyte. (C) Summary of the effects of β_{2b} on the surface expression of α_{1C} mutants. For each construct, the surface expression in the presence of β_{2b} was normalized to the average expression measured without β_{2b}. (D) The effect of β_{2b} on surface expression of α_{1C}-HA; panel a shows representative confocal images of whole oocytes, either native (uninjected) or expressing α_{1C}-HA + α_2/δ ("α_{1C}-HA") or α_{1C}-HA + α_2/δ + β_{2b} ("α_{1C}-HA+β_{2b}"). Injected RNA was 5 ng/oocyte. The dimensions of the image are 0.45 × 0.45 mm. The rightmost image exemplifies the method used to analyze the intensity of fluorescent labeling. A rectangle of a fixed width was superimposed on the image, and a profile of optical density (shown in b) along the axis approximately perpendicular to the PM (arrow) was obtained using the TINA software. (Optical density and distance were measured in arbitrary units inherent to the software). (b) Quantitative analysis of optical density profiles. The intensity was defined as the integral of the shaded area. The width of this area was defined as constant for all images taken in an experiment. The net intensity in each α_{1C}-HA–expressing oocyte was calculated by subtracting the average intensity measured in uninjected oocytes of the same experiment, and then normalized to the average net intensity of [α_{1C}-HA+α_2/δ]-expressing oocytes of this experiment. The normalized values, shown in c, were summarized across all experiments ($N = 3$).

of β_{2b} on $P_{o,max}$, instead of reducing it. This peculiar effect deserves further attention in the future.

The β_{2b}-induced increase in G_{max} still remaining after the elimination of the NTI module is comparable to the increase in the surface expression caused by β_{2b}. This indicates that in these mutants, the increase of the macroscopic Ca^{2+} channel conductance caused by β_{2b} may be the result of an increase in the amount of the functional channels, N, whereas $P_{o,max}$ is not substantially changed. This is illustrated by comparing the values of β-induced change in $P_{o,max}$ calculated using Eq. 6 (Table III).

The Initial Segment of the Short-NT Isoform of α_{1C} Is Not an NTI Module

Are aa 6–20 of long-NT sufficient to act as an NTI module? Does the initial segment of the short-NT isoform (aa 2–16) act as an inhibitory module, similarly to the partially homologous aa 6–20 segment in the long-NT? To answer these questions, we created a cDNA encoding for a short-NT isoform, α_{1C}-short, in which exon 1a of the long-NT was replaced by the exon 1 of short-NT α_{1C}

(Fig. 7 A). The rest of the molecule was left as in the cardiac, long-NT α_{1C}. This design was intended to single out the effects of NT and to avoid additional changes in channel's properties that can arise if one is using one of the several cloned short-NT isoforms, with additional variations in the other parts of the protein (Abernethy and Soldatov, 2002). We also created cDNAs encoding two chimeric proteins in which parts of short- and long-NT initial segments were switched (Fig. 7 A): (1) NT_{SL}, which is a short-NT α_{1C}, in which aa 2–16 of the short-NT α_{1C} are replaced by aa 6–20 of the long-NT α_{1C}; (2) NT_{LS}, which is a long-NT α_{1C} in which aa 6–20 are replaced by aa 2–16 of the short-NT. Two additional groups tested in these experiments included the standard $\alpha_{1C}\Delta46$ mutant (which misses the entire initial segment), and a new internal deletion of long-NT α_{1C}, $\alpha_{1C}\Delta21$-46. External HA-tagged constructs were also made for all new mutants except short-NT α_{1C}; they exhibited G-V curves and macroscopic I_{Ba} very similar to the untagged counterparts (Table I; unpublished data). Immunohistochemical measurements in giant membrane patches or in intact oocytes (for HA-tagged
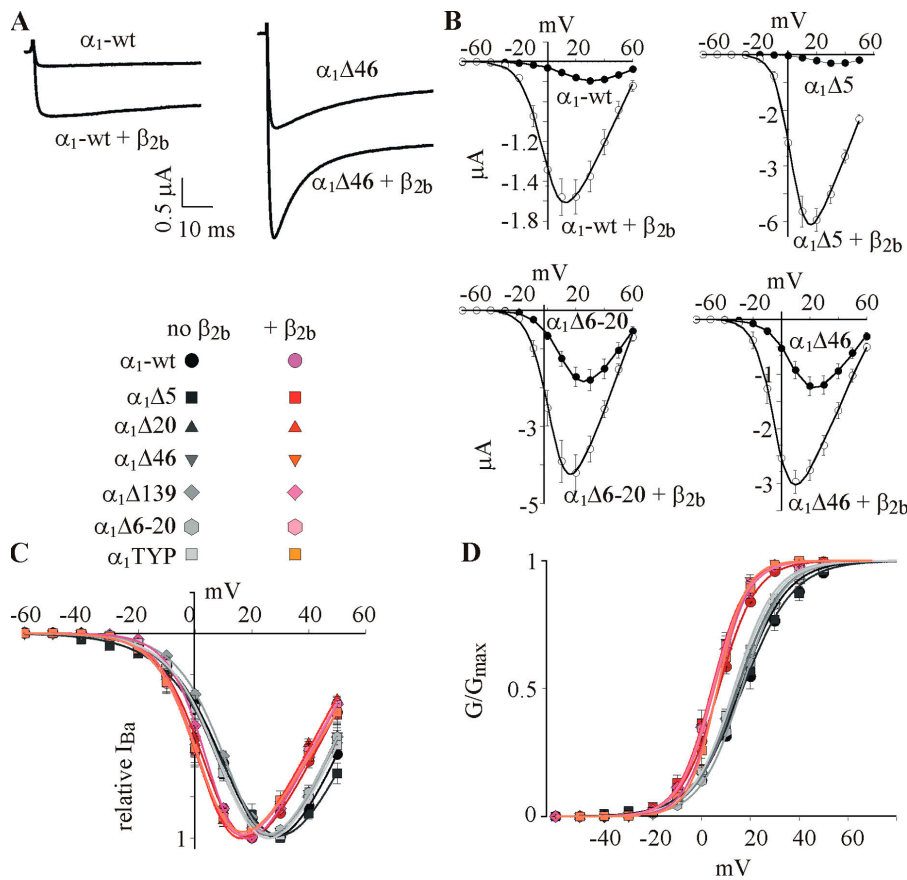
Figure 5. Effects of mutations in NT, and of the β_{2b} subunit, on voltage dependence of activation of I_{Ba}. (A) Representative net I_{Ba} of α_{1C}-wt and $\alpha_{1C}\Delta46$ constructs in the absence and presence of coexpressed β_{2b} subunit, recorded at +40 mV. (B) I-V curves of channels in $\alpha_1\alpha_2\delta$ and $\alpha_1\alpha_2\delta\beta_{2b}$ subunit compositions ($n = 6$–8, $N = 1$). Representative averaged I-V curves are shown for α_{1C}-wt, $\alpha_{1C}\Delta5$, $\alpha_{1C}\Delta6$-20, and $\alpha_{1C}\Delta46$. (C and D) Normalized averaged I-V curves (C) and G-V curves (D) from all experiments and all mutants tested, in absence (gray symbols) and presence (pink symbols) of the β_{2b} subunit. The solid lines were drawn for illustration using the Boltzmann equation with the averaged parameters of $V_{1/2}$ and K_a from Table I and V_{rev} from Table S1. Data are from 2–11 experiments, 14–56 cells.

constructs) showed that all new constructs expressed similarly to α_{1C}-wt in the PM, and coexpression of β_{2b} increased the amount of all constructs in the PM similarly to α_{1C}-wt (Fig. 7, B and C; Tables II and III).

Fig. 8 (A–C) reports on the results of two series of experiments (a and b) in which the macroscopic properties of I_{Ba} in the new constructs were tested, in different combinations and at two RNA doses. Without the β subunit, I_{Ba} in α_{1C}-short, NT_{SL}, and NT_{LS} was substantially greater than in α_{1C}-wt, and a small but significant leftward shift in $V_{1/2}$ and a decrease in K_a were also observed. All these parameters were comparable to those of $\alpha_{1C}\Delta46$ (Fig. 8; Tables I and II). I_{40} tended to be somewhat smaller in NT_{SL} than in α_{1C}-short or $\alpha_{1C}\Delta46$, but the difference did not reach statistical significance. In contrast, both macroscopic I_{Ba} and all G-V curve parameters of $\alpha_{1C}\Delta21$-46 were very similar to α_{1C}-wt.

Coexpression of β_{2b} shifted the G-V curve to the left by 12–17 mV in all constructs (Fig. 8 B; Table I), whereas the effects on I_{Ba} amplitude were again diverse. The increase in I_{40} caused by β_{2b} was poor (less than twofold) and comparable to $\alpha_{1C}\Delta46$ in α_{1C}-short and NT_{LS}, which lack the crucial 16 aa of the long-NT. In NT_{SL}, I_{40} increased much more than in $\alpha_{1C}\Delta46$ but less than in α_{1C}-wt, whereas $\alpha_{1C}\Delta21$-46 again behaved almost exactly as α_{1C}-wt (Fig. 8 C). The increase in $P_{o,max}$ caused by β_{2b} almost disappeared in $\alpha_{1C}\Delta46$ and NT_{LS} mutants; in the

α_{1C}-short, the calculation even showed a small decrease in $P_{o,max}$ by β_{2b} (Table III). In contrast, in NT_{SL}, the calculated $P_{o,max}$ was increased by β_{2b} almost like in the long-NT α_{1C}-wt. $\alpha_{1C}\Delta21$-46 behaved exactly like α_{1C}-wt (Fig. 8 Cb). Taken together, these results strongly suggest that aa 1–20 of long-NT fully restore the function of the NTI module, whereas aa 6–20 of long-NT alone are insufficient. aa 2–16 of short-NT cannot replace the homologous 15 aa of the long-NT as a crucial component of NTI module.

The difference in effects of β_{2b} on α_{1C}-wt and the various NT deletion mutants is further explored in Fig. 8 D, where the β_{2b}-induced increase in I_{Ba} at each voltage was normalized to that observed in α_{1C}-wt. The rationale for this analysis is as follows. If the NTI module regulates the effect of β_{2b} on $P_{o,max}$ (a nominally voltage-independent parameter) and not on the voltage dependence of activation, then the removal of the NTI module should alter the effect of β_{2b} to a similar extent at all voltages. In general, this was indeed the case (Fig. 8 D), although the relative effect of β_{2b} showed a slight voltage sensitivity; the difference between α_{1C}-wt and NT mutants was somewhat greater at more negative voltages. This, however, is a predictable consequence of the mild hyperpolarizing shift in the G-V curve caused by the removal of the NTI module (see Fig. 2 C and Fig. 8 B). The latter leads to a slightly stronger voltage dependency
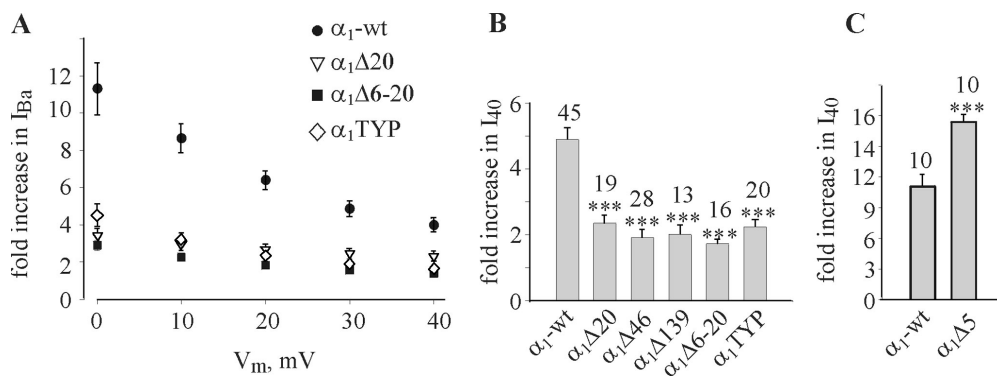
Figure 6. The NTI module regulates the effect of β_{2b} subunit. (A) The increase in I_{Ba} caused by coexpression of β_{2b} (relative to currents observed in the same α_{1C} constructs without β_{2b}) is much smaller in NT deletion mutants than in α_{1C}-wt, at all voltages. Shown are results of two representative experiments ($n = 10$–18). (B) A general summary of the effect of coexpression of β_{2b}. Shown is the fold increase in relative I_{40} in the various constructs; numbers of assayed cells are indicated above the bars. $N = 2$–7 experiments. (C) The increase in I_{Ba} caused by coexpression of β_{2b} is potentiated in the $\alpha_{1C}\Delta5$ mutant. $N = 2$.

of β_{2b}-induced increase in I_{Ba} in α_{1C}-wt than in the mutants. Fig. 8 D also illustrates the fact that, of all constructs tested, the increase in I_{Ba} by β_{2b} was the greatest in α_{1C}-wt and the smallest in α_{1C}-short (even compared with $\alpha_{1C}\Delta46$). The substantial recovery of the effect of β_{2b} in NT_{SL} and the full recovery in $\alpha_{1C}\Delta21$-46 are also clearly visualized.

DISCUSSION

Overview of Findings and Conclusions

Despite the importance of regulation of Ca^{2+} channels by β subunits and the wide interest in structure, function, and interactions of $Ca_v\alpha$ and $Ca_v\beta$, controversies still abound regarding the mechanisms and even the phenomenology of the effects of $Ca_v\beta$. In this study we attempt to sort out some of the discrepancies, and to better understand the mechanism by which $Ca_v\beta$ increases Ca^{2+} channel currents, focusing on a single type of $Ca_v\alpha_1$ and $Ca_v\beta$.

(a) We show that $Ca_v\beta$-induced increase in maximal open probability ($P_{o,max}$), at least in $Ca_v1.2$, is separable

from the other mechanisms (shift in G-V curve and change in PM expression) that underlie the increase in macroscopic Ca^{2+} currents by $Ca_v\beta$. This effect is crucially dependent on the presence of an NTI module. This separability, and the separability of trafficking from all gating effects, implies that $Ca_v\beta$ acts on α_{1C} to increase $P_{o,max}$ via molecular determinants (in β and/or in α_1) different from those used to change trafficking or to shift the G-V curve.

(b) Using deletion mutagenesis and chimeric constructs, we map the necessary and sufficient component of the NTI module to aa 1–20 of the long-NT and demonstrate that the NTI reduces $P_{o,max}$, thus restraining the activation of the channel at all voltages. Loss of NTI module enhances I_{Ba} by increasing $P_{o,max}$ $\sim$6–10-fold and, in parallel, specifically eliminates the effect of $Ca_v\beta$ on $P_{o,max}$; addition of the module restores the small amplitude of I_{Ba} and the enhancement of P_o by $Ca_v\beta$. This correlation supports the hypothesis (Shistik et al., 1998) that part of the effect of β on α_{1C} is due to a suppression of the inhibitory action of the NTI module. In the absence of the NTI module, $Ca_v\beta$ cannot further increase $P_{o,max}$, which is already high.

TABLE III

*Relative Changes in Surface Expression, G_{max}, I_{40}, and P_o Caused by Coexpression of β_{2b}*

Group	Fold increase in PM α_{1C} labeling	Fold increase in G_{max}	Fold increase in I_{40}	Fold increase in P_o from G_{max}	Fold increase in P_o from I_{40}
α_{1C}-wt	1.69 ± 0.19 (20; 4)	4.65 ± 0.39 (45; 7)	4.9 ± 0.37 (45; 7)	2.75	2.9
$\alpha_{1C}\Delta20$	1.65 ± 0.11 (11; 2)	2.48 ± 0.58[a] (19; 4)	2.36 ± 0.26[a] (19; 4)	1.5	1.43
$\alpha_{1C}\Delta46$	1.63 ± 0.08 (20; 3)	2.01 ± 0.22[a] (28; 5)	1.92 ± 0.23[a] (28; 5)	1.23	1.18
α_{1C}TYP	1.79 ± 0.04 (9; 2)	2.49 ± 0.21[a] (20; 3)	2.24 ± 0.23[a] (20; 3)	1.39	1.25
α_{1C}-short	1.64 ± 0.13 (12; 3)	1.25 ± 0.14[a] (11; 2)	1.31 ± 0.15[a] (11; 2)	0.76	0.8
NT_{SL}	1.58 ± 0.17 (9; 2)	4.12 ± 0.41 (16; 3)	4.07 ± 0.49 (16; 3)	2.6	2.57
HA-labeled constructs					
α_{1C}-HA	2.22 ± 0.21 (13; 1)	8.04 ± 0.93 (13; 3)	8.49 ± 1 (13; 3)	3.6	3.82
NT_{LS}-HA	1.99 ± 0.22 (7; 1)	2.36 ± 0.31[a] (9; 3)	2.29 ± 0.28[a] (9; 3)	1.18	1.15
$\alpha_{1C}\Delta21$-46-HA	2.86 ± 0.38 (11; 1)	10.9 ± 1.38 (12; 3)	11.03 ± 1.54 (12; 3)	3.8	3.85

All comparisons and normalization procedures are as in Table II.

[a]$P < 0.01$, compared with α_{1C}-wt.

A

```
α₁-wt      MLRALVQPAT PAYQPLPSHL SAETESTCKG TVVHEAQLNH FYISPGGSNY GSPRPAHANM  60
α₁Δ46      M--------- ---------- ---------- ---------- ------GSNY GSPRPAHANM  15
α₁-short   M----VNENT RMYIPEENHQ ---------- ---------- ------GSNY GSPRPAHANM  30
NT_LS      MLRALVNENT RMYIPEENHQ SAETESTCKG TVVHEAQLNH FYISPGGSNY GSPRPAHANM  60
NT_SL      M----VQPAT PAYQPLPSHL ---------- ---------- ------GSNY GSPRPAHANM  30
α₁Δ21-46   MLRALVQPAT PAYQPLPSHL ---------- ---------- ------GSNY GSPRPAHANM  34
```
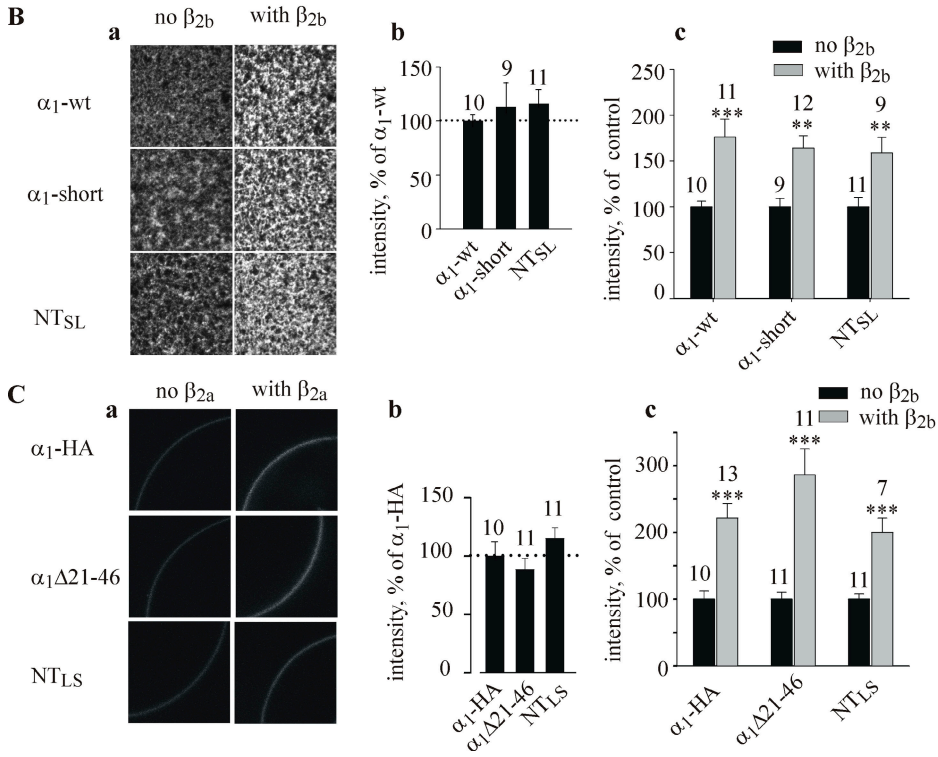

Figure 7. Design and surface expression of α_{1C}-short, short/long NT chimeras, and $\alpha_{1C}\Delta21$-46. (A) The design of initial NT segments of new constructs. Dashes show gaps. The homologous 15-aa sequence in long- and short-NT is highlighted in yellow and magenta, respectively. (B and C) Surface expression of the NT chimeric and deletion constructs in the absence and presence of β_{2b}, monitored in giant membrane patches (B) or in intact oocyte by imaging the external HA tag (C). The amount of injected RNA was 2.5 ng/oocyte in B and 5 ng in C. Examples of confocal images are shown in panel a, and the summary of the surface expression in the absence of β subunit (relative to α_{1C}-wt) is shown in b. The effect of coexpression of β_{2b} for each one of the constructs tested in these experiments is summarized in c. Numbers above bars indicate the number of patches (B) or oocytes (C) imaged.

(c) We establish that the NTI module is completely missing from a short-NT $Ca_v1.2$, which represents a class of $Ca_v1.2\alpha$ isoforms abundant in the smooth muscle and brain. This is a striking example of a physiologically meaningful disparate regulation of two very similar isoforms of an ion channel by an auxiliary subunit.

(d) Using two independent methods, we unequivocally demonstrate that coexpression of $Ca_v\beta$ increases the surface expression of α_{1C} in *Xenopus* oocytes approximately twofold, independently of the presence of the NTI module. By a critical examination of literature and separation of studies that used different NT isoforms, we resolve apparent controversies and single out remaining problems, regarding the effects of $Ca_v\beta$ on α_{1C}.

A Summary of the Effects of $Ca_v\beta$ on α_{1C}

It is known that the effects of β subunits differ among the various α_1 subunits (Dolphin, 2003). However, even for a single species of $Ca_v\alpha_1$, the details and magnitude of effects of coexpressed $Ca_v\beta$ often remain controversial. For instance, estimates of the increase in macroscopic maximal I_{Ba} of $Ca_v1.2$ (α_{1C}) in mammalian cells range between 15 and 20-fold (Lory et al., 1993; Takahashi et al., 2004) to almost no effect (Yasuda et al., 2004). The comparison between the different reports is thwarted by the unavoidable difference in recording conditions and often by an absence of quantitative estimates of some of the electrophysiological parameters. To understand the origins of the controversies, we summarized the data on $Ca_v\beta$ effects on $Ca_v1.2$ from reports that contain an explicit quantitative estimation of parameters that affect the macroscopic Ca^{2+} channel currents (Table IV). Data collected from short-NT (or mutants of α_{1C} missing the initial NT segment) and the long-NT isoforms of α_{1C} are separated. Macroscopic inactivation is unimportant in determining the whole-cell current when Ba^{2+} is used as the charge carrier (see below), and is left out of scope. Reports in which effects of different $Ca_v\beta$ have been compared but there are no data on channels expressed without $Ca_v\beta$ are not included. If several β subunits have been compared in the same study, we usually show β_{2a} or np-β_{2a} (β_{2b}), which were the most widely used. While the summary in Table IV may not be exhaustive, it is quite revealing.
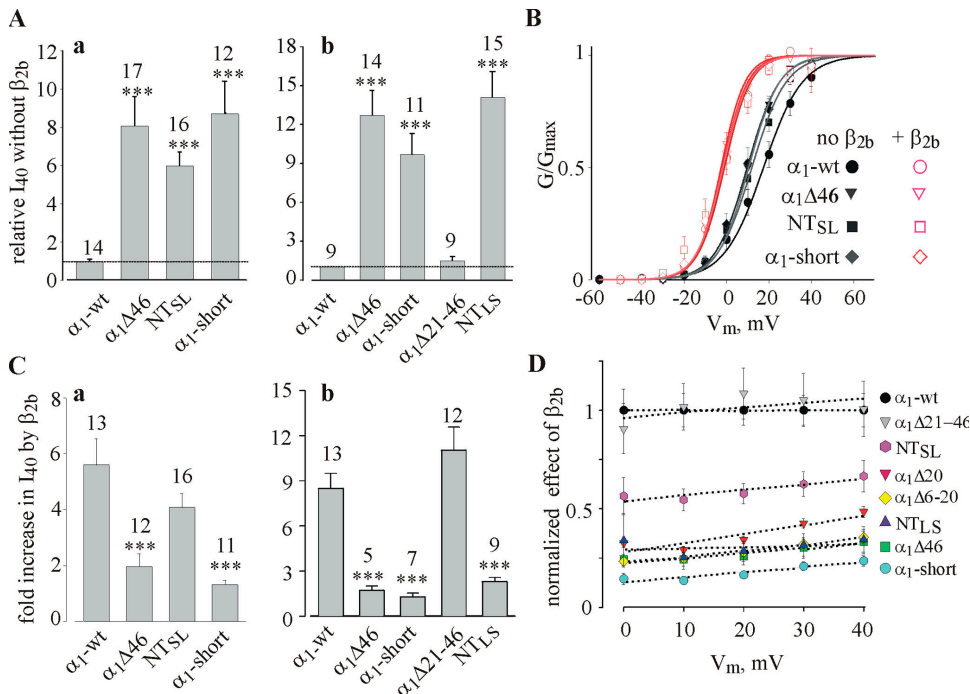
Figure 8. Chimeras of long- and short-NT help demarcate the NTI module. Two separate series of experiments, that used different doses of RNA, are shown in A–C. In Aa, B, and Ca, all RNAs were injected at 1 ng/oocyte; in Ab and Cb, at 2.5 ng/oocyte. (A) Comparison of normalized I_{40} in the absence of coexpressed β subunit. $N = 2$–3. (B) Effect of $β_{2b}$ on the voltage dependency of I_{Ba} in the same experiments as in Aa. Normalized averaged G-V curves are shown, in the absence (black symbols) and presence (red symbols) of the $β_{2b}$ subunit. (C) Summary of the effect of coexpression of $β_{2b}$ on I_{40}. (D) The voltage dependency of the relative effects of $β_{2b}$ on I_{Ba} in selected NT mutants. The results were summarized from experiments shown in Figs. 6 B and 8. In each experiment, the increase in I_{Ba} caused by the coexpression of $β_{2b}$ was normalized to the average increase observed in $α_{1C}$-wt group of oocytes at the same voltage, and the results were averaged across all experiments. The linear regression (dotted lines) is shown for illustrative purposes.

A Distinction between P_o and $P_{o,max}$

Whole-cell Ca^{2+} channel currents and/or conductance (G) depend both on the amount of functional channels (N) and on the open probability, P_o, such that $G = γ × N × P_o$, and $G_{max} = γ × N × P_{o,max}$ (see Materials and Methods, Eqs. 4 and 5). Treatments used in our experiments (NT deletions or coexpression of $β_{2b}$) do not affect γ (Shistik et al., 1995, 1998; Hullin et al., 2003), thus only N and P_o were changing. N is voltage independent, and assessing the impact of changes in N (once monitored) on G is straightforward.

In comparison, the analysis of P_o and the assessment of its effect on G are not trivial. First, in voltage-dependent channels, P_o is voltage dependent, being described by the same Boltzmann equation as G/G_{max} (Hille, 2002) (Eq. 3). P_o ranges from zero at negative potentials to $P_{o,max}$ at "saturating" membrane voltages where the G-V curve reaches a plateau. Note that in this classical treatment G_{max} and $P_{o,max}$ are voltage independent. An agent that improves the coupling between gating charge movement and pore opening, such as $Ca_vβ$ (Neely et al., 1993), and shifts the G-V curve to the left will increase P_o (and macroscopic currents) in a range of "nonsaturating" voltages, whether $P_{o,max}$ is changed or not. In contrast, an increase in $P_{o,max}$ leads to an increase in Ca^{2+} conductance at all voltages except those at which the channel is fully shut. Therefore, to understand the molecular mechanism of β's actions, it is important to distinguish between changes in P_o caused by a G-V curve shift vs. an increase in $P_{o,max}$.

In single-channel recordings it is possible to directly determine P_o, which is the fraction of time that a channel spends in open state(s), out of total observation time (Colquhoun and Sigworth, 1995). Although estimation of P_o can be distorted by the presence of inactivated states (Colquhoun and Sigworth, 1995), in $Ca_v1.2$ with Ba^{2+} as charge carrier, the inactivation is slow, and such distortion can be avoided by using short analyzed time segments (a few tens of milliseconds). Unfortunately, the estimation of changes in $P_{o,max}$ caused by $Ca_vβ$ is almost impossible in single-channel recording of Ca_v channels. Most publications report single channel currents recorded between −10 and +10 mV in high-Ba^{2+} solutions, to ensure high signal-to-noise ratio; a full I-V curve is usually not constructed. (An exception is a study in cardiomyocytes [Colecraft et al., 2002], where a full I-V relation was explored; see Table IV.) Under these conditions, G (and thus P_o) is very far from reaching a maximum, as evident from typical G-V curves shown in Figs. 2, 5, and 8, and the measured P_o does not provide any estimate of $P_{o,max}$.

In comparison, measurements of changes in macroscopic G_{max} in conjunction with a reliable estimation of N should provide a good measure of relative changes in $P_{o,max}$ (Wei et al., 1994; Takahashi et al., 2004). Here, G/G_{max} is calculated using the values of peak macroscopic current that are independent of the duration of voltage step, therefore the latter does not affect the calculated relative change in $P_{o,max}$. Our estimates of $P_{o,max}$ were not affected by changes in the steady-state

inactivation curve in the NT deletion mutants, because the availability of the channels for opening at the holding potential of -80 mV remained 100% (Shistik et al., 1998). There are two possible sources of inaccuracy. First, acceleration of the inactivation process by β_{2b} may decrease peak I_{Ba}, if the rate constants of activation and inactivation are comparable (Aldrich et al., 1983; Hille, 2002). However, this artifact is probably negligible in $Ca_v1.2$. Here, the time constant of the faster of the two components of macroscopic VDI of I_{Ba} is ~75 ms for a short-NT isoform (Shi and Soldatov, 2002) and >150 ms with the long-NT α_{1C} (unpublished data). This is at least twofold slower than first latency time constant observed in single channel recordings (~25–35 ms, see Hullin et al., 2003). Another artifact may arise when G_{max} is estimated by fitting experimental I-V curves to Boltzmann equation. In this case, G usually appears to reach its maximum at $+40$ to $+50$ mV. G-V curves based on the measurement of tail currents, which are devoid of certain inaccuracies inherent to I-V curves (such as very small I_{Ba} at V_m close to the reversal potential), often imply that the G-V curve has two components and does not reach a plateau at $+40$ to $+50$ mV, but close to 100 mV (e.g., Takahashi et al., 2004). Assuming that this is the case and using the data from Takahashi et al. (2004), we calculated that we might have overestimated the changes in G_{max}, but by no more than 30% (unpublished data). Since in α_{1C}-wt the changes in G_{max} caused by NT deletions or by β_{2b} are between 260 and 770% (Tables II and III), such an error would not affect our main conclusions.

$Ca_v\beta$-induced Changes in Voltage Dependency (G-V curve) and in $P_{o,max}$ Are Separable

(a) Only the $Ca_v\beta$-induced increase in $P_{o,max}$, but not the shift in G-V curve, depends on the presence of the NTI module. In all mutants lacking the crucial part of the NTI module (aa 6–20 of long NT), G-V curve shifts are like in α_{1C}-wt, but $P_{o,max}$ is not changed by β_{2b} (Table III). The mild approximately twofold increase in G_{max} (or I_{40}) caused by β_{2b} in these mutants can be almost fully accounted for by the increase in N, which is 1.6–2.2-fold. Strikingly, in the short-NT isoform, the coexpression of β_{2b} even causes an ~20% decrease in calculated P_o, despite a well-pronounced threefold increase in I_{Ba} at 0 mV (a V_m relevant for comparison with single-channel records). This increase is undoubtedly governed by the increase in N (see below) and the leftward shift in the G-V curve.

Published results (Table IV) fully support our data; separation of long-NT and short-NT isoforms eliminates controversies and allows solid conclusions. Coexpression of β subunits increases the P_o measured in single-channel patches at -10 to $+10$ mV in high-Ba^{2+}, in oocytes and in mammalian cells. However, the increase is consistently greater in the long-NT isoform

(range: six to eightfold) than in the short-NT α_{1C} forms (range: two to fivefold). Data necessary for the calculation of the relative change in $P_{o,max}$ are available from fewer works, but also fit our results; coexpression of $Ca_v\beta$ increases $P_{o,max}$ of the long-NT α_{1C} two to fourfold, whereas a mild ~20% decrease is observed in a short-NT α_{1C} isoform.

(b) Changes in $P_{o,max}$ caused by coexpression of $Ca_v\beta$ are similar in *Xenopus* oocytes and mammalian cells (Table IV). In contrast, there is a consistent and striking difference in the reported shifts in the G-V curve: changes in $\Delta V_{1/2}$ range from 12 to 22 mV in oocytes but are always <10 mV in mammalian cells. This intriguing difference calls for study and may provide new clues to understanding VDCC gating; but it also supports the disparity of mechanisms of the effects of $Ca_v\beta$ on $P_{o,max}$ and on voltage dependence of activation.

On the basis of these arguments, we conclude that, most intriguingly, the two gating actions of $Ca_v\beta$ that are most important in determining the amplitude of whole-cell Ca^{2+} currents are separable, and therefore may rely on distinct molecular mechanisms. It is remarkable that one of the most prominent actions of $Ca_v\beta$ can be selectively eliminated by removing a short segment of α_{1C} that does not even bind β, whereas other functions of $Ca_v\beta$ remain unchanged. This finding provides a hint at how a single $Ca_v\beta$ may regulate several different functions of α_1, without the need to assume the involvement of multiple β subunits.

Changes in Surface Expression Caused by β_{2b}

Surface expression of voltage-dependent ion channels can be gauged by quantitative immunohistochemistry of various kinds, or by measuring the maximal nonlinear gating charge movement, Q_{max}. The immunohistochemical methods that use monitoring of external surface-exposed parts of channel with or without genetically introduced epitopes reliably monitor the total number of channels in PM (e.g., Zerangue et al., 1999; Altier et al., 2002; Canti et al., 2005; Leroy et al., 2005) but do not guarantee that all detected channels are conducting (functional). Similarly, Q_{max} reflects the displacement of the voltage sensors in all channels in the PM, whether conducting or not. Relative changes in number of channel (N) caused by a regulatory factor (e.g., $Ca_v\beta$) are faithfully reflected in changes of either surface labeling or Q_{max}; however, the latter is also altered by factors that alter the charge or movement of the voltage sensors (Aggarwal and MacKinnon, 1996; Barrett et al., 2005).

The prevailing view is that the $Ca_v\beta$-induced increase in the amount of α_{1C} in the PM, reproducibly observed in mammalian cells including even cardiomyocytes (Table IV), does not occur in *Xenopus* oocytes. This notion is based on the reported absence of a significant $Ca_v\beta$-induced increase in Q_{max} measured in the oocytes using

TABLE IV

A Summary of Published Quantitative Analyses of the Effects of Coexpression of $Ca_v\beta$ Subunits on $Ca_v1.2$ Channels in Heterologous Expression Systems

A. Short-NT isoforms of α_{1C}										
Surface expression (fold increase)		$\Delta V_{1/2}$ (mV)		$P_{o,max}$ (fold increase)		P_o at −10 to 0 mV (fold increase)		Type of β	Type of α_{1C}[l]	Reference
Oocyte	Mamm cells	Oocyte	Mamm cells	Oocyte	Mamm cells	Oocyte	Mamm cells			
						1.9		β_3	Schultz	Wakamori et al., 1993
	4.8[a]		0		0.83[a]			β_3	Schultz	Josephson and Varadi, 1996
∼3[c,e]		16						β_3[d]	Schultz	Yamaguchi et al., 1998[b]
3.25[e]		19.5						β_{2a}	Schultz	Yamaguchi et al., 2000[b]
3.05[e]		18.4						β_{2a}	Schultz	Yamaguchi et al., 2000
							2–3[f]	β_{2a}	Biel	Hohaus et al., 2000
							5.2[f]	β_{2b}	Biel	Hullin et al., 2003
1.14		22						β_{1b}[d]	ΔN60[k]	Neely et al., 2004[b]
			1					β_{1b}	Snutch	Yasuda et al., 2004
			4–5					β_{2a}	Snutch	Yasuda et al., 2004
1.6		12		0.76				β_{2b}	See text	This report
B. Long-NT isoforms of α_{1C}										
Surface expression (fold increase)		$\Delta V_{1/2}$ (mV)		P_o,max (fold increase)		P_o at −10 to 0 mV (fold increase)		Type of β	Type of α_{1C}[l]	Reference
Oocyte	Mamm cells	Oocyte	Mamm cells	Oocyte	Mamm cells	Oocyte	Mamm cells			
		5						β_{1a}	Mikami	Wei et al., 1991[b]
	3.4[g]							β_{2a}	Mikami	Perez Reyes et al., 1992[b]
1.2[a]		16.6		4.3[a]				β_{2a}	Mikami	Neely et al., 1993[b]
		20						β_{2a}	Mikami	Neely et al., 1994
			5.2					β_3	Mikami	Lacinova et al., 1995
	11[g]							β_{1a}	Mikami	Perez Garcia et al., 1995
1.2–1.54[h]						8		β_{2b}	Mikami	Shistik et al., 1995
0.9–1.2[h]								β_{2b}	Mikami	Shistik et al., 1995[b]
	3.7[a]		0		2.5[a]			β_{1a}	Mikami[m]	Kamp et al., 1996
			6–10				8	β_{1a}, β_{2a}	Mikami[m]	Gerster et al., 1999[b]
	1.85[a]		1.5		2.6[j]			β_{2a}	cardiac[j]	Colecraft et al., 2002[j]
							6.4[f]	β_{2b}	Mikami	(Hullin et al., 2003)
	6.7[a]				2[a]			β_{2a}	Mikami	Takahashi et al., 2004
	7–8[i]		6.3				∼6	β_{1b}	Mikami[m]	Cohen et al., 2005[b]
1.7–2.7		14		2.75–3.6				β_{2b}	Mikami	This report

Surface expression, I-V shift, and P_o are usually presented for $\alpha_{1c}+\alpha_2\delta+\beta$ subunit combination vs. $\alpha_{1c}+\alpha_2\delta$, unless indicated otherwise. Mammalian cells were derivatives of HEK, COS, or similar cell lines lacking significant amounts of an endogenous α_{1C}. In one study (Colecraft et al., 2002), β subunits were overexpressed in cardiac myocytes.

[a]Changes in N were measured from Q_{max}. We have calculated $P_{o,max}$ using Eq. 6 and the presented data.

[b]No $\alpha_2\delta$ present.

[c]Estimated from current increase at peak, by comparing early (1 h) and late times after the injection of the β_3 protein; the shift in I-V is already complete by 1 h, and the difference in peak current is only due to surface expression (see Fig. 4 in Yamaguchi et al., 1998).

[d]Purified β protein was injected into oocytes.

[e]By imaging an intracellular HA tag added to α_{1C} at the NT. Oocytes were permeabilized with Triton-X100 and stained with an anti-HA antibody.

[f]In the presence of a dihydropyridine agonist.

[g]From total membrane [^{3}H]PN200-110 binding. This method does not exclude the labeling of α_{1C} located in ER or Golgi.

[h]Both by immunoprecipitation of α_{1C} from separated PM and by counting channels in cell-attached patches.

[i]By counting channels in patches. Measurement by surface biotinylation confirmed the increase in N, but there is no quantitative estimate.

[j]β_{2a} was overexpressed in cardiomyocytes on the background of existing cardiac channels, probably the long-NT α_{1C} type (Blumenstein et al., 2002; Pang et al., 2003). $P_{o,max}$ was measured in single channel records at +40 mV.

[k]A deletion mutant of the rabbit long-NT α_{1C} missing the first 60 aa.

[l]The types of α_{1C} are defined as follows: Mikami (Mikami et al., 1989) is the first cloned long-NT. This is the rabbit cardiac isoform, used also in the present study (termed α_{1C}-wt). Identical or nearly identical cDNAs were later cloned by Wei et al. (1991), Biel et al. (1991) and Lory et al. (1993).[m] Schultz (Schultz et al., 1993) is a human α_{1C} bearing 93% similarity to Mikami's clone but missing the first 59 aa at the NT (the protein starts with Met_{60} encoded by the first in-frame ATG of exon 2). Biel (Biel et al., 1990) is a rabbit lung short-NT α_{1C} with the 16-aa initial segment, and variations in a few downstream exons compared to Mikami's clone. Snutch (Snutch et al., 1991) is a short-NT (16 aa initial segment) rat cDNA; the most widely used is the rbII clone.

[m]The cDNA is identical to that of Mikami et al. (1989) except for an alternative exon encoding for a part of IVS3.

the cut-open voltage clamp, in which gating and ionic currents are measured from a large part of an internally perfused cell (Neely et al., 1993, 2004). In contrast, Yamaguchi et al. (1998, 2000) reported a threefold increase in α_{1C} caused in *Xenopus* oocytes by either injecting a purified β_3 subunit or by coexpressing β_{2a}. Although imaging of an intracellular HA tag in permeabilized oocytes, used in these works to monitor surface expression of α_{1C}, does not exclude the labeling of α_{1C} located in submembrane ER, the approximately threefold increase is also supported by observing the enhancement of I_{Ba} at different times after the injection of the β_3 protein (Yamaguchi et al., 1998; see Table IV legend for details). We have previously detected a β_{2b}-induced, 20–55% increase in N measured by counting channels in cell-attached patches and by immunoprecipitating α_{1C} from manually separated PM (Shistik et al., 1995), but it did not reach statistical significance. Interestingly, in the absence of $\alpha_2\delta$, even this small increase was not observed (Table IV).

To address the controversy and to measure changes in surface expression of α_{1C} in oocytes as accurately as possible, in this work we employed two additional, independent methods: immunolabeling of α_{1C}, tagged by an extracellular HA epitope, in whole oocytes; and imaging of immunolabeled α_{1C} in giant membrane patches of oocytes. Both methods clearly demonstrated a reproducible, highly statistically significant, isoform-independent increase in PM expression of α_{1C} induced by coexpression of β_{2b}. The estimates obtained by the widely accepted external tag measurement were slightly but usually insignificantly greater than by imaging in giant patches, when measured with the same construct of the channel (2.2-fold vs. 1.7-fold increase in α_{1C}-wt, respectively). We conclude that β_{2b} causes an approximately twofold increase in the PM content of α_{1C}, in the presence of $\alpha_2\delta$. The reason for the discrepancy with Neely et al. (1993, 2004) remains unclear; it would be interesting to see whether a change in Q_{max} occurs when $\alpha_2\delta$ is present. The increase in surface expression caused by coexpression $Ca_v\beta$ is absolutely independent of NTI module, in sharp contrast with $P_{o,max}$. These results corroborate the previously demonstrated separability of the effects of $Ca_v\beta$ on surface expression and gating (Canti et al., 1999, 2001; Gerster et al., 1999).

The NTI Module and the Effect of $Ca_v\beta$

In this report we demonstrated that α_{1C} variants lacking the NTI module (the various mutants and the short NT isoform) express in the PM at the same level as the long-NT isoform, though they give much larger macroscopic currents. These and our previous results (Shistik et al., 1998) firmly establish the role of the initial segment of long-NT as a regulator of gating, rather than expression, of α_{1C}. In support, Agler et al. (2005) recently found that the NT also constitutes an inhibitory module in the

N-type ($Ca_v2.2$) channel; in contrast to $Ca_v1.2$, in $Ca_v2.2$ the inhibitory effect of the NT is G protein gated.

Since the main effect of NTI is to regulate the voltage-independent parameter $P_{o,max}$, it is possible that the removal of the NTI module causes a modal shift in gating, like $Ca_v\beta$ (Costantin et al., 1998; Colecraft et al., 2002). If NTI module "tonically" restrains the opening of the channel's gate at all voltages (Shistik et al., 1998), its removal would cause a voltage-independent transition from a low-P_o mode to a high-P_o mode, in which the voltage independent transition from the last closed to the open state is more favorable than in the low-P_o mode. The slight change in the voltage dependence of activation in NT mutants lacking the NTI module may be due to a reequilibration among closed states, the transitions between which are voltage dependent. Further studies including single channel recordings will be required to test this conjecture.

We find that aa 6–20 constitute a crucial and necessary part of the inhibitory module; its deletion causes a maximal enhancement of $P_{o,max}$ and an almost complete disappearance of the enhancing effect of β_{2b} on $P_{o,max}$. Nevertheless, aa 6–20 alone only partially recover the function of the NTI when added at the NH_2 terminus of a $\alpha_{1C}\Delta46$ mutant, which lacks all 46 initial amino acid residues (NT_{SL} chimera). Full recovery of both functions of NTI (reduction in $P_{o,max}$ and enhancement of β_{2b}-induced increase in $P_{o,max}$) is achieved by the addition of aa 1–20 of the long-NT, which is thus established as a necessary and sufficient structural determinant of the NTI module. The function of aa 21–46, which link between the NTI module and the beginning of the highly conserved part of NT encoded by exon 2, is unknown at present. Our data conclusively demonstrate that the initial 16-aa NT segment of the short α_{1C} isoform is not an inhibitory module. These 16 aa were unable to restore the NTI functions even in the context of a full 46-aa initial segment, i.e., in the presence of aa 2–5 and 21–46 of the long NT (NT_{LS} chimera).

The interacting partners of NT in $Ca_v1.2$ are unknown. The regulation of inactivation kinetics of α_{1C} ($Ca_v1.2\alpha$) by β_{2a} involves voltage-dependent rearrangements of NT regions of α_{1C} and β_{2a}, as deduced from fluorescent resonance energy transfer (FRET) experiments (Kobrinsky et al., 2004). However, no physical interaction between NT of α_{1C} and $Ca_v\beta$ could be detected by direct biochemical measurements (Pragnell et al., 1994; Shistik et al., 1998), and the exact molecular interaction underlying the proximity between the NT of α_{1C} and β_{2a} indicated by FRET is yet to be determined. No direct interaction of NT with L1 (which would explain the intensive interplay with $Ca_v\beta$ function) could be detected in α_{1C} (Agler et al., 2005). Another possible interactor is the CT of α_{1C}. Similarly to NT, CT acts to prevent channel opening (Wei et al., 1994; Klockner et al., 1995; Gao et al., 2001; Mikala et al., 2003). Joint removal of NT

and distal CT causes a more-than-additive increase in I_{Ba} (Ivanina et al., 2000), suggesting that the relaxed state of the channel is a high-P_o one, and the termini are vital to prevent uncontrolled entry of Ca^{2+}.

Using *Xenopus* Oocytes vs. Mammalian Cells to Study the Effects of $Ca_v\beta$ on Ca^{2+} Channels

The validity of conclusions regarding $Ca_v\beta$ effects, especially changes in surface expression, obtained in *Xenopus* oocytes has often been met with reservations, because of the presence of an endogenous β subunit. However, HEK cells also contain endogenous β (Leroy et al., 2005). In this work we demonstrate that all major effects of $Ca_v\beta$ can be reproducibly observed and reliably studied in *Xenopus* oocytes. The $Ca_v\beta$-induced increase in surface α_{1C} in oocytes is in qualitative agreement with that in mammalian systems, although quantitatively the increase reported in mammalian cells is usually greater, more than fivefold (Table IV; but see Yasuda et al., 2004). The variability among different cell types may reflect variable levels of endogenous $Ca_v\beta$. The changes in gating parameters are also at least qualitatively (shift in G-V curve; see above) and quantitatively (change in $P_{o,max}$) similar.

Physiological Significance

$Ca_v1.2$ channels are crucial for contraction of cardiac and smooth muscles, hormone secretion, and regulation of gene expression in the brain (Reuter, 1983; Finkbeiner and Greenberg, 1998; Catterall, 2000; West et al., 2001; Lipscombe et al., 2004). In humans, the $Ca_v1.2$ gene, *CACNA1C* (Soldatov, 1994) contains 55 exons, of which 19 are subject to alternative splicing, giving rise to a very large number of isoforms (Tang et al., 2004). The exact exon combinations underlying the isoforms of α_{1C} in different tissues are yet to be catalogued (Abernethy and Soldatov, 2002; Jurkat-Rott and Lehmann-Horn, 2004; Tang et al., 2004). Long-NT isoform (isoforms?) is predominant in the heart but is also present in the brain, short-NT isoforms prevail in smooth muscle and brain (Slish et al., 1989; Koch et al., 1990; Snutch et al., 1991; Shistik et al., 1999; Blumenstein et al., 2002; Dai et al., 2002; Saada et al., 2003). At present we cannot exclude the possibility that in some of the short-NT isoforms of α_{1C} the function of the NT initial segment is different than in the isoform that we used here, due to an interaction with some alternative distant parts of α_{1C}; this remains to be investigated.

The isoforms may substantially differ in their physiological and pharmacological properties. For instance, splice variations in the COOH-terminal region regulate the inactivation of the channel and its sensitivity to certain pharmacological agents (Abernethy and Soldatov, 2002). The present work reveals a strikingly disparate regulation of two very similar isoforms of a Ca_v channel by a $Ca_v\beta$ subunit. It is notable that, in addition to the two isoforms of α_{1C} corresponding to splice variants with the alternative first exons 1 and 1a, another short-NT isoform lacking either of these exons and starting from exon 2 may exist in human tissues (Schultz et al., 1993; Saada et al., 2003). This would correspond to the truncation mutant $\alpha_{1C}\Delta46$ or, if the protein starts with the first methionine of exon 2, to $\alpha_{1C}\Delta59$ (see Fig. 1). The differences in function of NH_2 termini of these isoforms, discovered in this paper, are expected to have significant physiological implications. They will result in substantial differences in amplitudes of macroscopic Ca^{2+} currents and in the effects of $Ca_v\beta$ (whose association with α_1 may change in development and growth; see Spafford et al., 2004) or regulators that act in a $Ca_v\beta$-dependent manner, such as protein kinase A (Bunemann et al., 1999).

REFERENCES

Abernethy, D.R., and N.M. Soldatov. 2002. Structure-functional diversity of human L-type Ca^{2+} channel: perspectives for new pharmacological targets. *J. Pharmacol. Exp. Ther.* 300:724–728.

Aggarwal, S.K., and R. MacKinnon. 1996. Contribution of the S4 segment to gating charge in the Shaker K^+ channel. *Neuron.* 16:1169–1177.

Agler, H.L., J. Evans, L.H. Tay, M.J. Anderson, H.M. Colecraft, and D.T. Yue. 2005. G protein-gated inhibitory module of N-type ($Ca_v2.2$) Ca^{2+} channels. *Neuron.* 46:891–904.

Aldrich, R.W., D.P. Corey, and C.F. Stevens. 1983. A reinterpretation of mammalian sodium channel gating based on single channel recording. *Nature.* 306:436–441.

Altier, C., S.J. Dubel, C. Barrere, S.E. Jarvis, S.C. Stotz, R.L. Spaetgens, J.D. Scott, V. Cornet, M. DeWaard, G.W. Zamponi, et al. 2002. Trafficking of L-type calcium channels mediated by the postsynaptic scaffolding protein AKAP79. *J. Biol. Chem.* 277:33598–33603.

Barrett, C.F., Y.Q. Cao, and R.W. Tsien. 2005. Gating deficiency in a familial hemiplegic migraine type 1 mutant P/Q-type calcium channel. *J. Biol. Chem.* 280:24064–24071.

Bichet, D., V. Cornet, S. Geib, E. Carlier, S. Volsen, T. Hoshi, Y. Mori, and M. De Waard. 2000. The I-II loop of the Ca^{2+} channel $\alpha1$ subunit contains an endoplasmic reticulum retention signal antagonized by the β subunit. *Neuron.* 25:177–190.

Biel, M., R. Hullin, S. Freundner, D. Singer, N. Dascal, V. Flockerzi, and F. Hofmann. 1991. Tissue-specific expression of high-voltage-activated dihydropyridine-sensitive L-type calcium channels. *Eur. J. Biochem.* 200:81–88.

Biel, M., P. Ruth, E. Bosse, R. Hullin, W. Stuhmer, V. Flockerzi, and F. Hofmann. 1990. Primary structure and functional expression of a high voltage activated calcium channel from rabbit lung. *FEBS Lett.* 269:409–412.

Birnbaumer, L., N. Qin, R. Olcese, E. Tareilus, D. Platano, J. Costantin, and E. Stefani. 1998. Structures and functions of calcium channel β subunits. *J. Bioenerg. Biomembr.* 30:357–375.

Blumenstein, Y., N. Kanevsky, G. Sahar, R. Barzilai, T. Ivanina, and N. Dascal. 2002. A novel long-N-terminus isoform of human L-type Ca^{2+} channel is up-regulated by protein kinase C. *J. Biol. Chem.* 277:3419–3423.

Brice, N.L., N.S. Berrow, V. Campbell, K.M. Page, K. Brickley, I. Tedder, and A.C. Dolphin. 1997. Importance of the different β subunits in the membrane expression of the α_{1A} and α_2 calcium channel subunits: studies using a depolarization-sensitive α_{1A} antibody. *Eur. J. Neurosci.* 9:749–759.

Bunemann, M., B.L. Gerhardstein, T. Gao, and M.M. Hosey. 1999. Functional regulation of L-type calcium channels via protein kinase A-mediated phosphorylation of the β2 subunit. *J. Biol. Chem.* 274:33851–33854.

Canti, C., A. Davies, N.S. Berrow, A.J. Butcher, K.M. Page, and A.C. Dolphin. 2001. Evidence for two concentration-dependent processes for β-subunit effects on α_{1B} calcium channels. *Biophys. J.* 81:1439–1451.

Canti, C., M. Nieto-Rostro, I. Foucault, F. Heblich, J. Wratten, M.W. Richards, J. Hendrich, L. Douglas, K.M. Page, A. Davies, and A.C. Dolphin. 2005. The metal-ion-dependent adhesion site in the Von Willebrand factor-A domain of $\alpha_2\delta$ subunits is key to trafficking voltage-gated Ca^{2+} channels. *Proc. Natl. Acad. Sci. USA.* 102:11230–11235.

Canti, C., K.M. Page, G.J. Stephens, and A.C. Dolphin. 1999. Identification of residues in the N terminus of α_{1B} critical for inhibition of the voltage-dependent calcium channel by Gβγ. *J. Neurosci.* 19:6855–6864.

Castellano, A., X. Wei, L. Birnbaumer, and E. Perez Reyes. 1993. Cloning and expression of a neuronal calcium channel β subunit. *J. Biol. Chem.* 268:12359–12366.

Catterall, W.A. 2000. Structure and regulation of voltage-gated Ca^{2+} channels. *Annu. Rev. Cell Dev. Biol.* 16:521–555.

Chen, Y.H., M.H. Li, Y. Zhang, L.L. He, Y. Yamada, A. Fitzmaurice, Y. Shen, H. Zhang, L. Tong, and J. Yang. 2004. Structural basis of the α1-β subunit interaction of voltage-gated Ca^{2+} channels. *Nature.* 429:675–680.

Chien, A.J., K.M. Carr, R.E. Shirokov, E. Rios, and M.M. Hosey. 1996. Identification of palmitoylation sites within the L-type calcium channel β_{2a} subunit and effects on channel function. *J. Biol. Chem.* 271:26465–26468.

Chien, A.J., T. Gao, E. Perez Reyes, and M.M. Hosey. 1998. Membrane targeting of L-type calcium channels. Role of palmitoylation in the subcellular localization of the β_{2a} subunit. *J. Biol. Chem.* 273:23590–23597.

Chien, A.J., X. Zhao, R.E. Shirokov, T.S. Puri, C.F. Chang, D. Sun, E. Rios, and M.M. Hosey. 1995. Roles of a membrane-localized β subunit in the formation and targeting of functional L-type Ca^{2+} channels. *J. Biol. Chem.* 270:30036–30044.

Chu, P.-J., J.K. Larsen, C.-C. Chen, and P.M. Best. 2004. Distribution and relative expression levels of calcium channel β subunits within the chambers of the rat heart. *J. Mol. Cell. Cardiol.* 36:423–434.

Cohen, R.M., J.D. Foell, R.C. Balijepalli, V. Shah, J.W. Hell, and T.J. Kamp. 2005. Unique modulation of L-type Ca^{2+} channels by short auxiliary β_{1d} subunit present in cardiac muscle. *Am. J. Physiol.* 288: H2363–H2374.

Colecraft, H.M., B. Alseikhan, S.X. Takahashi, D. Chaudhuri, S. Mittman, V. Yegnasubramanian, R.S. Alvania, D.C. Johns, E. Marban, and D.T. Yue. 2002. Novel functional properties of Ca^{2+} channel β subunits revealed by their expression in adult rat heart cells. *J. Physiol.* 541:435–452.

Colquhoun, D., and F.J. Sigworth. 1995. Fitting and statistical analysis of single-channel records. *In* Single-channel Recording.

B. Sakmann and E. Neher, editors. Plenum Press, New York. pp. 483–587.

Costantin, J., F. Noceti, N. Qin, X. Wei, L. Birnbaumer, and E. Stefani. 1998. Facilitation by the β_{2a} subunit of pore openings in cardiac Ca^{2+} channels. *J. Physiol.* 507:93–103.

Dai, B., N. Saada, C. Echetebu, C. Dettbarn, and P. Palade. 2002. A new promoter for α_{1C} subunit of human L-type cardiac calcium channel $Ca_v1.2$. *Biochem. Biophys. Res. Commun.* 296:429–433.

Dalton, S., S.X. Takahashi, J. Miriyala, and H.M. Colecraft. 2005. A single $Ca_v\beta$ can reconstitute both trafficking and macroscopic conductance of voltage-dependent calcium channels. *J. Physiol.* 567:757–769.

Dascal, N. 1987. The use of *Xenopus* oocytes for the study of ion channels. *CRC Crit. Rev. Biochem.* 22:317–387.

Dascal, N., and I. Lotan. 1992. Expression of exogenous ion channels and neurotransmitter receptors in RNA-injected *Xenopus* oocytes. *In* Protocols in Molecular Neurobiology. Volume 13. A. Longstaff and P. Revest, editors. Humana Press, Totowa, NJ. pp. 205–225.

Dascal, N., I. Lotan, E. Karni, and A. Gigi. 1992. Calcium channel currents in *Xenopus* oocytes injected with rat skeletal muscle RNA. *J. Physiol.* 450:469–490.

De Waard, M., C.A. Gurnett, and K.P. Campbell. 1996. Structural and functional diversity of voltage-activated calcium channels. *Ion Channels.* 4:41–87.

Dolphin, A.C. 2003. β subunits of voltage-gated calcium channels. *J. Bioenerg. Biomembr.* 35:599–620.

Ertel, E.A., K.P. Campbell, M.M. Harpold, F. Hofmann, Y. Mori, E. Perez-Reyes, A. Schwartz, T.P. Snutch, T. Tanabe, L. Birnbaumer, et al. 2000. Nomenclature of voltage-gated calcium channels. *Neuron.* 25:533–535.

Finkbeiner, S., and M.E. Greenberg. 1998. Ca^{2+} channel-regulated neuronal gene expression. *J. Neurobiol.* 37:171–189.

Gao, T., A.J. Chien, and M.M. Hosey. 1999. Complexes of the α_{1C} and β subunits generate the necessary signal for membrane targeting of class C L-type calcium channels. *J. Biol. Chem.* 274:2137–2144.

Gao, T., A.E. Cuadra, H. Ma, M. Bunemann, B.L. Gerhardstein, T. Cheng, R. Ten Eick, and M.M. Hosey. 2001. C-terminal fragments of the α_{1C} ($Ca_v1.2$) subunit associate with and regulate L-type calcium channels containing C-terminally truncated α_{1C} subunits. *J. Biol. Chem.* 276:21089–21097.

Garcia, R., E. Carrillo, S. Rebolledo, M.C. Garcia, and J.A. Sanchez. 2002. The β1a subunit regulates the functional properties of adult frog and mouse L-type Ca^{2+} channels of skeletal muscle. *J. Physiol.* 545:407–419.

Gerster, U., B. Neuhuber, K. Groschner, J. Striessnig, and B.E. Flucher. 1999. Current modulation and membrane targeting of the calcium channel α_{1C} subunit are independent functions of the β subunit. *J. Physiol.* 517:353–368.

Gregg, R.G., A. Messing, C. Strube, M. Beurg, R. Moss, M. Behan, M. Sukhareva, S. Haynes, J.A. Powell, R. Coronado, and P.A. Powers. 1996. Absence of the β subunit (cchb1) of the skeletal muscle dihydropyridine receptor alters expression of the α_1 subunit and eliminates excitation-contraction coupling. *Proc. Natl. Acad. Sci. USA.* 93:13961–13966.

Harry, J.B., E. Kobrinsky, D.R. Abernethy, and N.M. Soldatov. 2004. New short splice variants of the human cardiac $Ca_v\beta_2$ subunit: redefining the major functional motifs implemented in modulation of the $Ca_v1.2$ channel. *J. Biol. Chem.* 279:46367–46372.

Hille, B. 2002. Ion Channels of Excitable Membranes. Sinauer, Sunderland, MA. 722 pp.

Hohaus, A., M. Poteser, C. Romanin, N. Klugbauer, F. Hofmann, I. Morano, H. Haase, and K. Groschner. 2000. Modulation of the smooth-muscle L-type Ca^{2+} channel α1 subunit (α_{1C-b}) by the β2a subunit: a peptide which inhibits binding of β to the I-II

linker of α1 induces functional uncoupling. *Biochem. J.* 348(Pt 3): 657–665.

Hullin, R., I.F. Khan, S. Wirtz, P. Mohacsi, G. Varadi, A. Schwartz, and S. Herzig. 2003. Cardiac L-type calcium channel β-subunits expressed in human heart have differential effects on single channel characteristics. *J. Biol. Chem.* 278:21623–21630.

Hullin, R., D. Singer-Lahat, M. Freichel, M. Biel, N. Dascal, F. Hofmann, and V. Flockerzi. 1992. Calcium channel β subunit heterogeneity: functional expression of cloned cDNA from heart, aorta and brain. *EMBO J.* 11:885–890.

Isom, L.L., K.S. De Jongh, and W.A. Catterall. 1994. Auxiliary subunits of voltage-gated ion channels. *Neuron.* 12:1183–1194.

Ivanina, T., Y. Blumenstein, E. Shistik, R. Barzilai, and N. Dascal. 2000. Modulation of L-type Ca^{2+} channels by Gβγ and calmodulin via interactions with N- and C-termini of $α_{1C}$. *J. Biol. Chem.* 275:39846–39854.

Jones, S.W. 2002. Calcium channels: when is a subunit not a subunit? *J. Physiol.* 545:334.

Josephson, I.R., and G. Varadi. 1996. The β subunit increases Ca^{2+} currents and gating charge movements of human cardiac L-type Ca^{2+} channels. *Biophys. J.* 70:1285–1293.

Jurkat-Rott, K., and F. Lehmann-Horn. 2004. The impact of splice isoforms on voltage-gated calcium channel α1 subunits. *J. Physiol.* 554:609–619.

Kamp, T.J., M.T. Perez Garcia, and E. Marban. 1996. Enhancement of ionic current and charge movement by coexpression of calcium channel $β_{1A}$ subunit with $α_{1C}$ subunit in a human embryonic kidney cell line. *J. Physiol.* 492:89–96.

Klockner, U., G. Mikala, M. Varadi, G. Varadi, and A. Schwartz. 1995. Involvement of the carboxyl-terminal region of the α1 subunit in voltage-dependent inactivation of cardiac calcium channels. *J. Biol. Chem.* 270:17306–17310.

Kobrinsky, E., K.J. Kepplinger, A. Yu, J.B. Harry, H. Kahr, C. Romanin, D.R. Abernethy, and N.M. Soldatov. 2004. Voltage-gated rearrangements associated with differential β-subunit modulation of the L-type Ca^{2+} channel inactivation. *Biophys. J.* 87:844–857.

Koch, W.J., P.T. Ellinor, and A. Schwartz. 1990. cDNA cloning of a dihydropyridine-sensitive calcium channel from rat aorta. Evidence for the existence of alternatively spliced forms. *J. Biol. Chem.* 265:17786–17791.

Lacinova, L., A. Ludwig, E. Bosse, V. Flockerzi, and F. Hofmann. 1995. The block of the expressed L-type calcium channel is modulated by the β3 subunit. *FEBS Lett.* 373:103–107.

Leroy, J., M.S. Richards, A.J. Butcher, M. Nieto-Rostro, W.S. Pratt, A. Davies, and A.C. Dolphin. 2005. Interaction via a key tryptophan in the I-II linker of N-type calcium channels is required for β1 but not for palmitoylated β2, implicating an additional binding site in the regulation of channel voltage-dependent properties. *J. Neurosci.* 25:6984–6996.

Leuranguer, V., E. Bourinet, P. Lory, and J. Nargeot. 1998. Antisense depletion of β subunits fails to affect T-type calcium channels properties in a neuroblastoma cell line. *Neuropharmacology.* 37:701–708.

Liman, E.R., J. Tytgat, and P. Hess. 1992. Subunit stoichiometry of a mammalian K^+ channel determined by construction of multimeric cDNAs. *Neuron.* 9:861–871.

Lipscombe, D., T.D. Helton, and W. Xu. 2004. L-type calcium channels: the low down. *J. Neurophysiol.* 92:2633–2641.

Lory, P., G. Varadi, D.F. Slish, M. Varadi, and A. Schwartz. 1993. Characterization of β subunit modulation of a rabbit cardiac L-type Ca^{2+} channel $α_1$ subunit as expressed in mouse L cells. *FEBS Lett.* 315:167–172.

Maltez, J.M., D.A. Nunziato, J. Kim, and G.S. Pitt. 2005. Essential $Ca_vβ$ modulatory properties are AID-independent. *Nat. Struct. Mol. Biol.* 12:372–377.

McGee, A.W., D.A. Nunziato, J.M. Maltez, K.E. Prehoda, G.S. Pitt, and D.S. Bredt. 2004. Calcium channel function regulated by the SH3-GK module in β subunits. *Neuron.* 42:89–99.

Mikala, G., I. Bodi, U. Klockner, M. Varadi, G. Varadi, S.E. Koch, and A. Schwartz. 2003. Characterization of auto-regulation of the human cardiac α1 subunit of the L-type calcium channel: importance of the C-terminus. *Mol. Cell. Biochem.* 250:81–89.

Mikami, A., K. Imoto, T. Tanabe, T. Niidome, Y. Mori, H. Takeshima, S. Narumiya, and S. Numa. 1989. Primary structure and functional expression of the cardiac dihydropyridine-sensitive calcium channel. *Nature.* 340:230–233.

Mori, Y., T. Friedrich, M.S. Kim, A. Mikami, J. Nakai, P. Ruth, E. Bosse, F. Hofmann, V. Flockerzi, T. Furuichi, et al. 1991. Primary structure and functional expression from complementary DNA of a brain calcium channel. *Nature.* 350:398–402.

Namkung, Y., S.M. Smith, S.B. Lee, N.V. Skrypnyk, H.L. Kim, H. Chin, R.H. Scheller, R.W. Tsien, and H.S. Shin. 1998. Targeted disruption of the Ca^{2+} channel $β_3$ subunit reduces N- and L-type Ca^{2+} channel activity and alters the voltage-dependent activation of P/Q-type Ca^{2+} channels in neurons. *Proc. Natl. Acad. Sci. USA.* 95:12010–12015.

Neely, A., J. Garcia-Olivares, S. Voswinkel, H. Horstkott, and P. Hidalgo. 2004. Folding of active calcium channel $β_{1b}$ subunit by size-exclusion chromatography and its role on channel function. *J. Biol. Chem.* 279:21689–21694.

Neely, A., R. Olcese, X. Wei, L. Birnbaumer, and E. Stefani. 1994. Ca^{2+}-dependent inactivation of a cloned cardiac Ca^{2+} channel $α_1$ subunit ($α_{1C}$) expressed in *Xenopus* oocytes. *Biophys. J.* 66:1895–1903.

Neely, A., X. Wei, R. Olcese, L. Birnbaumer, and E. Stefani. 1993. Potentiation by the β subunit of the ratio of the ionic current to the charge movement in the cardiac calcium channel. *Science.* 262:575–578.

Olcese, R., N. Qin, T. Schneider, A. Neely, X. Wei, E. Stefani, and L. Birnbaumer. 1994. The amino terminus of a calcium channel β subunit sets rates of channel inactivation independently of the subunit's effect on activation. *Neuron.* 13:1433–1438.

Opatowsky, Y., C.C. Chen, K.P. Campbell, and J.A. Hirsch. 2004. Structural analysis of the voltage-dependent calcium channel β subunit functional core and its complex with the α1 interaction domain. *Neuron.* 42:387–399.

Pang, L., G. Koren, Z. Wang, and S. Nattel. 2003. Tissue-specific expression of two human $Ca_v1.2$ isoforms under the control of distinct 5′ flanking regulatory elements. *FEBS Lett.* 546:349–354.

Peleg, S., D. Varon, T. Ivanina, C.W. Dessauer, and N. Dascal. 2002. $Gα_i$ controls the gating of the G-protein-activated K^+ channel, GIRK. *Neuron.* 33:87–99.

Perez Garcia, M.T., T.J. Kamp, and E. Marban. 1995. Functional properties of cardiac L-type calcium channels transiently expressed in HEK293 cells. Roles of $α_1$ and β subunits. *J. Gen. Physiol.* 105:289–305.

Perez Reyes, E., A. Castellano, H.S. Kim, P. Bertrand, E. Baggstrom, A.E. Lacerda, X.Y. Wei, and L. Birnbaumer. 1992. Cloning and expression of a cardiac/brain β subunit of the L-type calcium channel. *J. Biol. Chem.* 267:1792–1797.

Pragnell, M., M. De Waard, Y. Mori, T. Tanabe, T.P. Snutch, and K.P. Campbell. 1994. Calcium channel β subunit binds to a conserved motif in the I-II cytoplasmic linker of the $α_1$ subunit. *Nature.* 368:67–70.

Qin, N., R. Olcese, J. Zhou, O.A. Cabello, L. Birnbaumer, and E. Stefani. 1996. Identification of a second region of the beta-subunit involved in regulation of calcium channel inactivation. *Am. J. Physiol.* 271:C1539–C1545.

Qin, N., D. Platano, R. Olcese, J.L. Costantin, E. Stefani, and L. Birnbaumer. 1998. Unique regulatory properties of the type 2a

Ca^{2+} channel β subunit caused by palmitoylation. *Proc. Natl. Acad. Sci. USA*. 95:4690–4695.

Reuter, H. 1983. Calcium channel modulation by neurotransmitters, enzymes and drugs. *Nature*. 301:569–574.

Saada, N., B. Dai, C. Echetebu, S.K. Sarna, and P. Palade. 2003. Smooth muscle uses another promoter to express primarily a form of human Ca$_V$1.2 L-type calcium channel different from the principal heart form. *Biochem. Biophys. Res. Commun.* 302:23–28.

Schreibmayer, W., H.A. Lester, and N. Dascal. 1994. Voltage clamp of *Xenopus laevis* oocytes utilizing agarose cushion electrodes. *Pflugers Arch.* 426:453–458.

Schultz, D., G. Mikala, A. Yatani, D.B. Engle, D.E. Iles, B. Segers, R.J. Sinke, D.O. Weghuis, U. Klockner, M. Wakamori, et al. 1993. Cloning, chromosomal localization, and functional expression of the α1 subunit of the L-type voltage-dependent calcium channel from normal human heart. *Proc. Natl. Acad. Sci. USA.* 90:6228–6232.

Sharon, D., D. Vorobiov, and N. Dascal. 1997. Positive and negative coupling of the metabotropic glutamate receptors to a G protein-activated K$^+$ channel, GIRK, in *Xenopus* oocytes. *J. Gen. Physiol.* 109:477–490.

Shi, C., and N.M. Soldatov. 2002. Molecular determinants of voltage-dependent slow inactivation of the Ca^{2+} channel. *J. Biol. Chem.* 277:6813–6821.

Shistik, E., T. Ivanina, Y. Blumenstein, and N. Dascal. 1998. Crucial role of N terminus in function of cardiac L-type Ca^{2+} channel and its modulation by protein kinase C. *J. Biol. Chem.* 273:17901–17909.

Shistik, E., T. Ivanina, T. Puri, M. Hosey, and N. Dascal. 1995. Ca^{2+} current enhancement by α$_2$/δ and β subunits in *Xenopus* oocytes: contribution of changes in channel gating and α$_1$ protein level. *J. Physiol.* 489:55–62.

Shistik, E., T. Keren-Raifman, G.H. Idelson, N. Dascal, and T. Ivanina. 1999. The N-terminus of the cardiac L-type Ca^{2+} channel α$_{1C}$ subunit: the initial segment is ubiquitous and crucial for protein kinase C modulation, but it is not directly phosphorylated. *J. Biol. Chem.* 274:31145–31149.

Singer, D., M. Biel, I. Lotan, V. Flockerzi, F. Hofmann, and N. Dascal. 1991. The roles of the subunits in the function of the calcium channel. *Science.* 253:1553–1557.

Singer-Lahat, D., N. Dascal, L. Mittelman, S. Peleg, and I. Lotan. 2000. Imaging plasma membrane proteins in large membrane patches of *Xenopus* oocytes. *Pflugers Arch.* 440:627–633.

Singer-Lahat, D., I. Lotan, M. Biel, V. Flockerzi, F. Hofmann, and N. Dascal. 1994. Cardiac calcium channels expressed in *Xenopus* oocytes are modulated by dephosphorylation but not by cAMP-dependent phosphorylation. *Receptors Channels.* 2:215–226.

Slish, D.F., D.B. Engle, G. Varadi, I. Lotan, D. Singer, N. Dascal, and A. Schwartz. 1989. Evidence for the existence of a cardiac specific isoform of the α1 subunit of the voltage dependent calcium channel. *FEBS Lett.* 250:509–514.

Snutch, T.P., W.J. Tomlinson, J.P. Leonard, and M.M. Gilbert. 1991. Distinct calcium channels are generated by alternative splicing and are differentially expressed in the mammalian CNS. *Neuron.* 7:45–57.

Soldatov, N.M. 1994. Genomic structure of human L-type Ca^{2+} channel. *Genomics.* 22:77–87.

Spafford, J.D., J. Van Minnen, P. Larsen, A.B. Smit, N.I. Syed, and G.W. Zamponi. 2004. Uncoupling of calcium channel α1 and β subunits in developing neurons. *J. Biol. Chem.* 279:41157–41167.

Stotz, S.C., and G.W. Zamponi. 2001. Structural determinants of fast inactivation of high voltage-activated Ca2+ channels. *Trends Neurosci.* 24:176–182.

Striessnig, J. 1999. Pharmacology, structure and function of cardiac L-type Ca^{2+} channels. *Cell. Physiol. Biochem.* 9:242–269.

Strube, C., M. Beurg, P.A. Powers, R.G. Gregg, and R. Coronado. 1996. Reduced Ca^{2+} current, charge movement, and absence of Ca^{2+} transients in skeletal muscle deficient in dihydropyridine receptor β1 subunit. *Biophys. J.* 71:2531–2543.

Takahashi, S.X., J. Miriyala, and H.M. Colecraft. 2004. Membrane-associated guanylate kinase-like properties of β-subunits required for modulation of voltage-dependent Ca^{2+} channels. *Proc. Natl. Acad. Sci. USA.* 101:7193–7198.

Takahashi, S.X., J. Miriyala, L.H. Tay, D.T. Yue, and H.M. Colecraft. 2005. A Ca$_V$β SH3/guanylate kinase domain interaction regulates multiple properties of voltage-gated Ca^{2+} channels. *J. Gen. Physiol.* 126:365–377.

Tang, Z.Z., M.C. Liang, S. Lu, D. Yu, C.Y. Yu, D.T. Yue, and T.W. Soong. 2004. Transcript scanning reveals novel and extensive splice variations in human L-type voltage-gated calcium channel, Ca$_V$1.2 α1 subunit. *J. Biol. Chem.* 279:44335–44343.

Tareilus, E., M. Roux, N. Qin, R. Olcese, J. Zhou, E. Stefani, and L. Birnbaumer. 1997. A *Xenopus* oocyte β subunit: evidence for a role in the assembly/expression of voltage-gated calcium channels that is separate from its role as a regulatory subunit. *Proc. Natl. Acad. Sci. USA.* 94:1703–1708.

Van Petegem, F., K.A. Clark, F.C. Chatelain, and D.L. Minor Jr. 2004. Structure of a complex between a voltage-gated calcium channel β subunit and an α subunit domain. *Nature.* 429:671–675.

Varadi, G., P. Lory, D. Schultz, M. Varadi, and A. Schwartz. 1991. Acceleration of activation and inactivation by the β subunit of the skeletal muscle calcium channel. *Nature.* 352:159–162.

Varadi, G., Y. Mori, G. Mikala, and A. Schwartz. 1995. Molecular determinants of Ca^{2+} channel function and drug action. *Trends Pharmacol. Sci.* 16:43–49.

Wakamori, M., G. Mikala, A. Schwartz, and A. Yatani. 1993. Single-channel analysis of a cloned human heart L-type Ca^{2+} channel α$_1$ subunit and the effects of a cardiac β subunit. *Biochem. Biophys. Res. Commun.* 196:1170–1176.

Walker, D., D. Bichet, S. Geib, E. Mori, V. Cornet, T.P. Snutch, Y. Mori, and M. De Waard. 1999. A new β subtype-specific interaction in α$_{1A}$ subunit controls P/Q-type Ca^{2+} channel activation. *J. Biol. Chem.* 274:12383–12390.

Walker, D., and M. De Waard. 1998. Subunit interaction sites in voltage-dependent Ca^{2+} channels: role in channel function. *Trends Neurosci.* 21:148–154.

Wei, S.-k., H.M. Colecraft, C.D. DeMaria, B.Z. Peterson, R. Zhang, T.A. Kohout, T.B. Rogers, and D.T. Yue. 2000. Ca^{2+} channel modulation by recombinant auxiliary β subunits expressed in young adult heart cells. *Circ. Res.* 86:175–184.

Wei, X., A. Neely, A.E. Lacerda, R. Olcese, E. Stefani, E. Perez Reyes, and L. Birnbaumer. 1994. Modification of Ca^{2+} channel activity by deletions at the carboxyl terminus of the cardiac α$_1$ subunit. *J. Biol. Chem.* 269:1635–1640.

Wei, X., A. Neely, R. Olcese, W. Lang, E. Stefani, and L. Birnbaumer. 1996. Increase in Ca^{2+} channel expression by deletions at the amino terminus of the cardiac α$_{1C}$ subunit. *Receptors Channels.* 4:205–215.

Wei, X.Y., E. Perez Reyes, A.E. Lacerda, G. Schuster, A.M. Brown, and L. Birnbaumer. 1991. Heterologous regulation of the cardiac Ca^{2+} channel α$_1$ subunit by skeletal muscle β and γ subunits. Implications for the structure of cardiac L-type Ca^{2+} channels. *J. Biol. Chem.* 266:21943–21947.

West, A.E., W.G. Chen, M.B. Dalva, R.E. Dolmetsch, J.M. Kornhauser, A.J. Shaywitz, M.A. Takasu, X. Tao, and M.E. Greenberg. 2001. Calcium regulation of neuronal gene expression. *Proc. Natl. Acad. Sci. USA.* 98:11024–11031.

Williams, M.E., D.H. Feldman, A.F. McCue, R. Brenner, G. Velicelebi, S.B. Ellis, and M.M. Harpold. 1992. Structure and functional

expression of α_1, α_2, and β subunits of a novel human neuronal calcium channel subtype. *Neuron.* 8:71–84.

Yamaguchi, H., M. Hara, M. Strobeck, K. Fukasawa, A. Schwartz, and G. Varadi. 1998. Multiple modulation pathways of calcium channel activity by a β subunit. Direct evidence of β subunit participation in membrane trafficking of the α_{1C} subunit. *J. Biol. Chem.* 273:19348–19356.

Yamaguchi, H., M. Okuda, G. Mikala, K. Fukasawa, and G. Varadi. 2000. Cloning of the β_{2a} subunit of the voltage-dependent calcium channel from human heart: cooperative effect of α_2/δ and β_{2a} on the membrane expression of the α_{1C} subunit. *Biochem. Biophys. Res. Commun.* 267:156–163.

Yasuda, T., L. Chen, W. Barr, J.E. McRory, R.J. Lewis, D.J. Adams, and G.W. Zamponi. 2004. Auxiliary subunit regulation of high-voltage activated calcium channels expressed in mammalian cells. *Eur. J. Neurosci.* 20:1–13.

Zerangue, N., B. Schwappach, Y.N. Jan, and L.Y. Jan. 1999. A new ER trafficking signal regulates the subunit stoichiometry of plasma membrane K_{ATP} channels. *Neuron.* 22:537–548.